Processing of second-order, contrast-modulated stimuli in mouse visual cortex

Dissertation

zur Erlangung des Grades eines
Doktors der Naturwissenschaften

der Mathematisch-Naturwissenschaftlichen Fakultät
und
der Medizinischen Fakultät
der Eberhard-Karls-Universität Tübingen

vorgelegt
von

Zeinab Khastkhodaei
aus Shiraz, Iran

März, 2017

Tag der mündlichen Prüfung: 16.03.2017

Dekan der Math.-Nat. Fakultät: Prof. Dr. W. Rosenstiel

Dekan der Medizinischen Fakultät: Prof. Dr. I. B. Autenrieth

1. Berichterstatter: Prof. Dr. / PD Dr. / Dr. Laura Busse

2. Berichterstatter: Prof. Dr. / PD Dr. / Dr. Thomas Euler

Prüfungskommission: Prof. Dr. / PD Dr. / Dr. Laura Busse

Prof. Dr. / PD Dr. / Dr. Thomas Euler

Prof. Dr. / PD Dr. / Dr. Uwe Ilg

Prof. Dr. / PD Dr. / Dr. Cornelius Schwrarz

Erklärung / Declaration:

Ich erkläre, dass ich die zur Promotion eingereichte Arbeit mit dem Titel:

„Processing of second-order, contrast-modulated stimuli in mouse visual cortex

.....“

selbständig verfasst, nur die angegebenen Quellen und Hilfsmittel benutzt und wörtlich oder inhaltlich übernommene Stellen als solche gekennzeichnet habe. Ich versichere an Eides statt, dass diese Angaben wahr sind und dass ich nichts verschwiegen habe. Mir ist bekannt, dass die falsche Abgabe einer Versicherung an Eides statt mit Freiheitsstrafe bis zu drei Jahren oder mit Geldstrafe bestraft wird.

I hereby declare that I have produced the work entitled "……", submitted for the award of a doctorate, on my own (without external help), have used only the sources and aids indicated and have marked passages included from other works, whether verbatim or in content, as such. I swear upon oath that these statements are true and that I have not concealed anything. I am aware that making a false declaration under oath is punishable by a term of imprisonment of up to three years or by a fine.

Tübingen, den 26.06.2017 Zeinab Khastkhodaei

Datum / Date Unterschrift /Signature

Table of Contents

Summary

Visual processing along the primate ventral stream takes place across a hierarchy of areas, characterized by an increase in both complexity of neuronal preferences and invariance to changes of low-level stimulus attributes. A basic type of invariance is form-cue invariance, where neurons have similar preferences in response to first-order stimuli, defined by changes in luminance, and global features of second-order stimuli, defined by changes in texture or contrast. Whether in mice, a now popular model system for early visual processing, visual perception can be guided by second-order stimuli is currently unknown.

In this project, we asked whether mice can use second-order stimuli to guide visual perception in a cue-invariant way and assessed potential cue-invariant representations of stimulus orientation in two areas of mouse visual cortex.

For both behavioral and electrophysiological experiments, we used a common set of luminance-modulated gratings (*LGs*) and contrast-modulated gratings (*CGs*), obtained by multiplying a contrast envelope with a noise carrier. We created two types of *CG* stimuli that differed in the Fourier energy distribution of the carrier: high-frequency noise and low-frequency noise. To examine a potential effect of different contrast of *LGs* and *CGs*, we matched the root-mean-square (RMS) contrast between first- and second-order gratings, in which case *c* was 0.335 for the *LGs*.

We tested whether mice can generalize orientation discrimination learned with first-order, *LGs* to various untrained second-order, *CGs*. We first trained head-fixed mice in a classical conditioning paradigm to perform a coarse orientation discrimination on *LGs*. Once the animal reached stable and reliable orientation discrimination performance, we replaced *LGs* with *CGs* with low-frequency noise carriers to test the generalization of orientation discrimination to second-order gratings. We found that mice, after learning a coarse orientation discrimination involving only *LGs*, could readily generalize orientation discrimination to *CGs*, albeit with a substantial drop in performance. Then, we wondered whether the overall lower performance for *CGs* was related to their lower RMS contrast compared with *LGs*. To test this hypothesis, we probed mice with *LGs* whose RMS contrast was lowered to match that of *CGs*. We found that mice could perform well during the orientation discrimination task for *LGs* matched in RMS contrast. Indeed, across all animals tested, performance was similar for both levels of contrast. Finally, we tested mice with *CGs* with high-frequency noise carriers. Again, mice could see this type of *CG* and importantly, they could also discriminate between the two grating orientations, albeit performance was again considerably lower compared with that for *LGs*. Together, these results demonstrate that mice can use second-order stimuli to guide visual perception.

We performed extracellular recordings, both during anesthesia and wakefulness, in mouse areas V1 and LM, where we compared orientation tuning curves to *LGs* and *CGs*. We found that neurons in area V1 and LM were less responsive and less selective to *CGs* than to *LGs*, both during anesthesia and wakefulness. Interestingly, this reduction was particularly prominent during anesthesia. We wondered whether our finding of weaker responses and broader orientation tuning for *CG* than *LG* responses could be explained by the lower RMS contrast of *CGs*. Thus, we performed control experiments, in which we measured responses to *LGs* that were matched in RMS contrast to the *CGs*. We found that neurons in both visual areas still responded more weakly to *CGs* than *LGs* but this reduction in responsiveness was less pronounced compared with conditions with full

contrast *LGs*. Similar to our results with full-contrast *LGs*, orientation selectivity also decreased considerably between *LGs* matched in RMS contrast and *CGs*. Indeed, orientation selectivity did not differ significantly between responses to full-contrast and reduced-contrast *LGs*. Together, the reduced RMS contrast of *CGs* might contribute to the reduction in peak responsiveness to *CGs* but cannot account for the poorer orientation selectivity for *CGs*. We also investigated the underlying mechanism of responses to second-order stimuli in awake recordings: we tested orientation tunings of both V1 and area LM in response to a high-frequency noise *CGs*, in which the noise carrier's spatial frequency distribution was concentrated beyond the passband of many V1 and LM neurons (Marshel et al., 2011). We first observed that less than half of the recorded neurons with significant responses to *LGs* also had visually evoked activity to *CGs* with high-frequency noise. This fraction of responsive neurons was considerably lower compared to that obtained for *CGs* with low-frequency noise. Interestingly, the difference in responsiveness between the two types of *CG* stimuli was stronger for area V1 than LM. To examine whether the *CG* representation might contribute toward cue-invariant perception of stimulus orientation, we also compared the neurons' preferred orientation, separately for each grating type. We found that preferred orientations for *CGs* with low-frequency noise and *LGs* were correlated for both areas V1 and LM. Interestingly, for *CGs* with high-frequency noise, the distribution of differences in preferred orientation was non-uniform only for area LM and preferred orientations were only correlated for area LM. Together, the broad similarity of preferred orientations between grating types provides some evidence for a coarse cue-invariance, which might in turn be part of the neural basis for perceptual generalization of orientation discrimination.

Introduction

Central visual pathways

The last 50 years have seen major advances in our understanding of the visual system, and in particular of the visual cortex. Responses of neurons in the mammalian visual cortex were first thoroughly quantified by Hubel and Wiesel, more than 50 years ago (Hubel and Wiesel, 1959). Today, we know that the processing of visual information is performed to a large extent in the visual cortex, which is subdivided into distinct areas: in the primate, there are approximately 32 separate neocortical areas involved in visual processing (Felleman and Van Essen, 1991). These areas are organized into two broadly segregated processing streams: the ventral stream for object recognition and the dorsal stream for object localization. Each stream consists of multiple areas beyond V1 and has V1 as a primary input source (Mishkin and Ungerleider, 1982; Ungerleider and Haxby, 1994) (**Figure 1**).

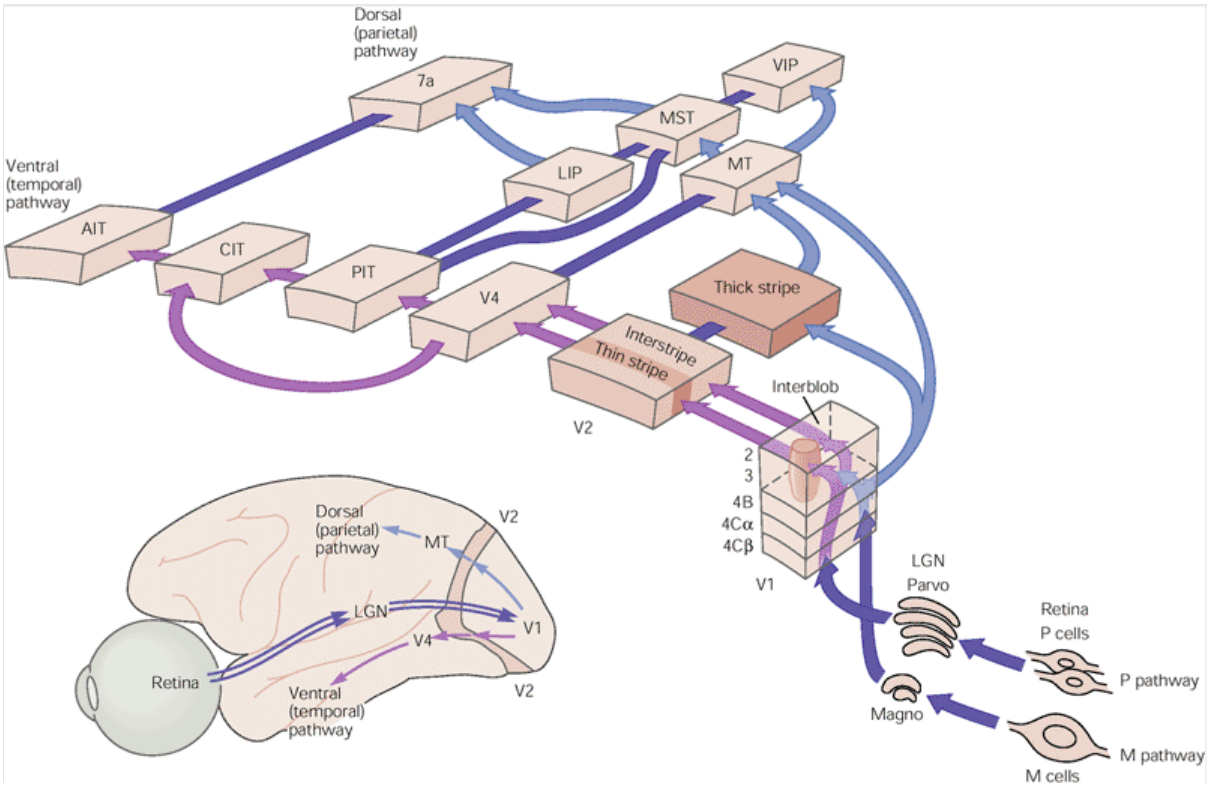

Figure 1. Two parallel pathways of visual processing in primates. (Adapted from Erik R. Kandel, Principles of Neural Sciences p.1164)

Hierarchy of visual processing

In primates, visual processing along the ventral stream takes place across a hierarchy of areas. In this hierarchy the complexity of neural preferences increases, such that V1 neurons prefer orientated edges (Hubel and Wiesel, 1959, 1962; De Valois et al., 1982), V2 neurons respond to contours, textures and combination of orientations (Anzai et al., 2007; Willmore et al., 2010; Freeman et al., 2013), V4 neurons process curvatures (Pasupathy and Connor, 1999) and finally neurons in IT, the final stage of the ventral

stream, prefer complex objects such as faces (Desimone et al., 1984; Logothetis and Sheinberg, 1996; Tanaka, 1996).
The selectivity of V1 neurons was reported, for the first time, by Hubel and Wiesel (Hubel and Wiesel, 1959). In the seminal experiments of Hubel and Wiesel, they discovered that cells in cat primary visual cortex tended to respond in one of two ways. The first group, which they termed "simple cells", responds more when the light is presented in a certain direction and these responses can be predicted based on the excitatory and inhibitory organization of their receptive fields. However, the second group, which they named "complex cells", does not have fixed inhibitory and excitatory subregions in their receptive fields and the direction selectivity of these neurons cannot be predicted based on their receptive fields organizations. One step further in the hierarchy, V2 neurons respond to combinations of similar and dissimilar orientations. The property of having different orientation preferences in receptive field subregions gives V2 neurons the capability to process curves and angles (Anzai et al., 2007), despite the fact V2 neurons do not show more than one peak in their orientation tuning curve when probed with bars or gratings. Further evidence for gradually increasing complexity comes from a study comparing V1 and V2 neuronal responses to natural images. Whereas most of V2 neurons respond to natural images stronger than to control stimuli, this modulation effect is minimal in V1 neurons (Freeman et al., 2013). V4 neurons process even more complicated visual features and prepare the information for shape recognition in the next stages. The modulation depth of V4 neurons by contour features is much stronger than by edges and bars. Moreover, a subpopulation of V4 neurons are selective for contour features and show a bias toward convex contours (Pasupathy and Connor, 1999). Finally, in IT, the final stage of ventral stream, neurons respond more to complex than simple images such that a subpopulation of IT neurons is specialized to recognize faces (Desimone et al., 1984; Logothetis and Sheinberg, 1996; Tanaka, 1996).

Gradually increasing invariance

Another example of increasing the complexity of visual information processing along ventral stream is the tolerance to changes in low-level stimulus features in object recognition. Previous studies have shown that IT neurons conserve their selectivity despite changes in position, scale and context of an image. As depicted in **Figure 2**, monkeys were shown different images, where each individual image varies in scale, position and context, and the ability of V4 and IT neurons to generalize their selectivity was tested. Many neurons in V4 and IT maintain their shape selectivity across changes in position, size and context (Schwartz et al., 1983; Rust and DiCarlo, 2010). Another study demonstrated that area IT, which has overlapping columns forming a continuous mapping of complex features, is able to produce the image of an object, invariant to different viewing angles and illumination conditions (Tanaka et al., 1996). Moreover, the tolerance increases as visual information travels from V4 to IT along ventral stream, and therefore neurons become more tolerant to changes in low-level stimulus attributes (Rust and DiCarlo, 2010) (**Figure 2**).

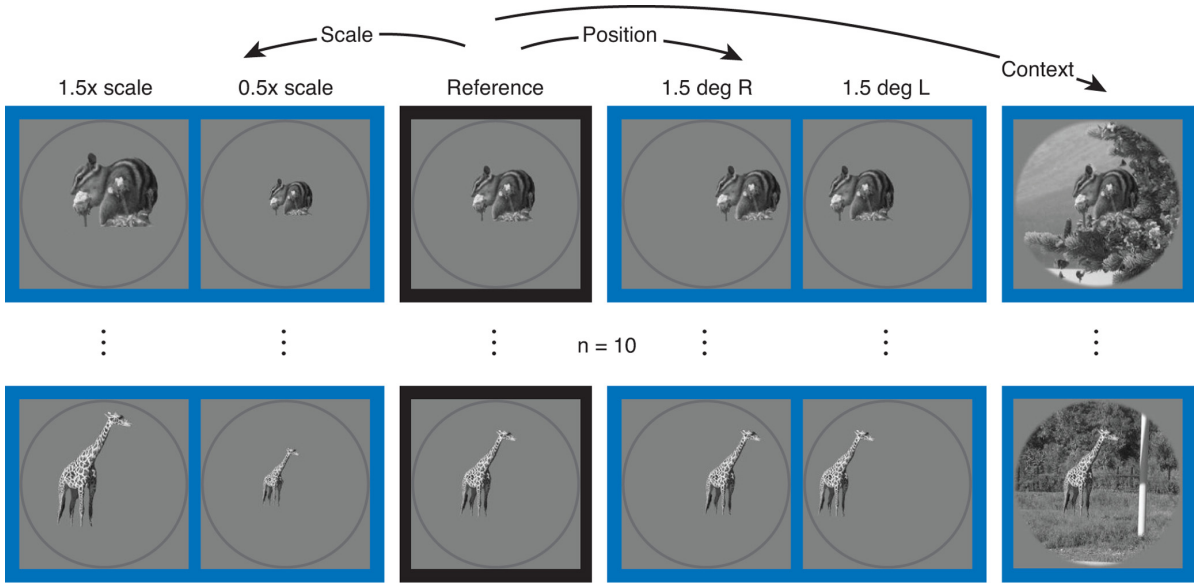

Figure 2. In the hierarchy of the ventral stream (e.g. in V4 and IT areas), neural selectivity is tolerant to changes in low-level visual features (Adapted from Rust and DiCarlo, 2010).

Form-cue invariance

One basic type of invariance is form-cue invariance (Baker and Mareschal, 2001), where neurons have similar preferences whether driven by first-order or second-order stimuli.

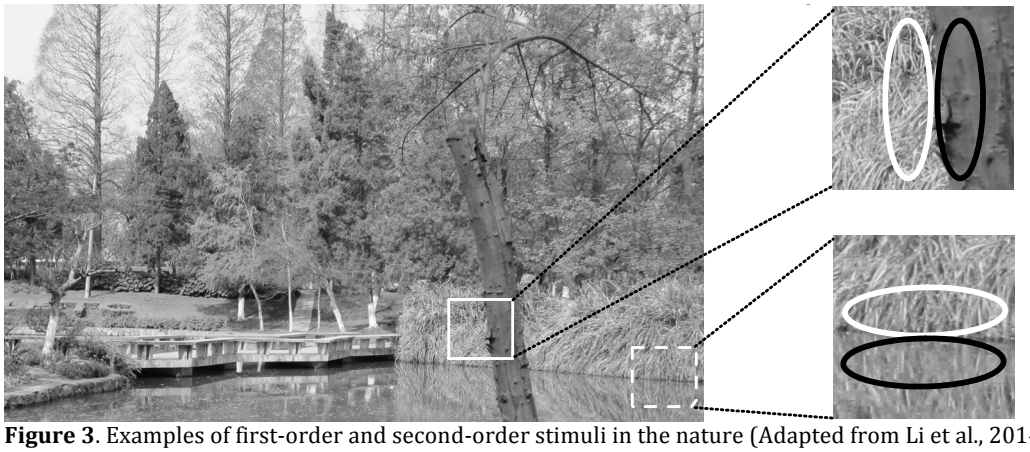

Figure 3. Examples of first-order and second-order stimuli in the nature (Adapted from Li et al., 2014)

First-order and second-order stimuli

In order to perform object recognition, our visual system needs to first analyze the local features of natural images, which are due to surface properties, illumination, and boundaries. It has been established that neurons in early visual system encode the local changes in luminance. However, there are other types of objects, which are segregated from their background with other cues than luminance and our visual system is still able to perceive them. In the natural image in **Figure 3**, we recognize the tree from the grassy background and the grass from its reflection in the water with two different mechanisms: in the first case the luminance is the local attribute change between tree and grassy background, whereas the grass is distinguished from its reflection by a difference in contrast. Those stimuli whose principal features are characterized by changes in luminance are referred to as first-order stimuli; sine wave gratings are a

common type of first-order stimuli and have been used in many studies. Visual stimuli, which are characterized by variations in other visual cues than luminance, such as contrast, texture and color are defined as second-order stimuli. By now, different types of second-order stimuli have been used to investigate second-order processing. **Figure 4** illustrates a few types of second-order stimuli. One of the most common types of second-order stimuli is a contrast-modulated grating (*CG*). *CGs* consist of two elements: a noise texture, called a carrier, and a low spatial frequency grating, called an envelope. In *CGs* the contrast of carrier changes by envelope.

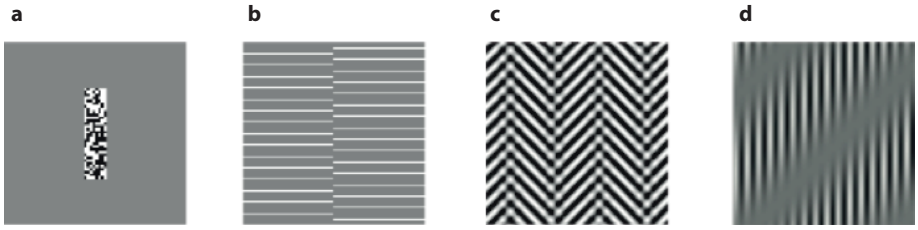

Figure 4. Examples of second-order stimuli used in previous studies. ***a***. Texture-defined bar. ***b***. Illusory contours. ***c***. Texture-defind gratings. ***d***. Contrast-modulated gratings (*CGs*).

Neuronal responses to second-order stimuli

Neural responses to second-order motion was reported first by Albright 1992, who showed that neurons in area MT/V5 have the same preferred direction to *LGs* and moving dynamic noise on a static noise background (Form-cue invariance) (Albright, 1992). So far, cue-invariant neurons have been observed in primate V2 (Li et al., 2014) (but see El-Shamayleh and Movshon, 2011; An et al., 2014), MT (Albright, 1992) and IT (Sary et al., 1993), and cat area 18 (Zhou and Baker, 1994; Leventhal et al., 1998; Mareschal and Baker, 1998a, b; Zhan and Baker, 2006; Song and Baker, 2007).

In most of these electrophysiological and anatomical studies, the second-order responsive neurons showed weaker responses to second-order than to first-order stimuli (Mareschal and Baker, 1998a; Zhan and Baker, 2006; Li et al., 2014). For instance, optical imaging in area 18 of cats has shown that the population responses to both contrast-contour and illusory-contour stimuli, which are two types of second-order stimuli, were approximately 20% of those to *LGs* (Zhan and Baker, 2006). Similar results have been obtained in electrophysiological studies conducted in monkeys and cats, such that only one-third of V2 neurons responded to *CGs* and these responses were weaker than those to first-order stimuli (Mareschal and Baker, 1998a; Li and Baker, 2012; Li et al., 2014). Therefore, cue-invariant neurons have been shown to be typically less responsive to second-order than to first-order stimuli.

The properties of both global and local features of second-order stimuli have been studied in details. Spatial frequency and orientation of both the carrier and the envelope have been shown to determine second-order responses. Furthermore, it has been shown that the ratio of carrier spatial frequency to envelope spatial frequency used to construct second-order stimuli, influences the probability of driving neurons with second-order stimuli. For example, applying various combinations of carrier and envelope spatial frequency demonstrated that different ratios of carrier spatial frequency to envelope spatial frequency (Zhou and Baker, 1994) instead of a fixed ratio (Albrecht and Hamilton, 1982) increases the probability of driving neurons with second-order stimuli. Furthermore, the spatial frequency tuning measurements of the

carrier have revealed that second-order responsive neurons prefer higher carrier spatial frequencies, and although the preferred ratio of carrier spatial frequency to envelope spatial frequency differs across neurons, this ratio tends to be around 8 (Li et al., 2014) (**Figure 5**). However, there is no fixed relationship between carrier and envelope spatial frequency and the preferred spatial frequency for the envelope is similar to that of *LGs* (Zhan and Baker, 2006; Li et al., 2014).

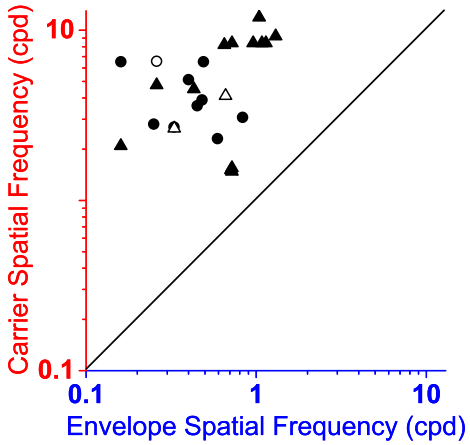

Figure 5. The preferred spatial frequencies of the carrier (red) are around 8 times than those for the envelope (blue). Triangles represent neurons with complex-type responses and circles represent neurons with simple-type responses. For more details see Li et al., 2014. (Adapted from Li et al., 2014).

Another feature of second-order stimuli that has been investigated in detail is the carrier and envelope orientations. Previous studies have demonstrated that envelope orientation is the main factor of second-order responses (Mareschal and Baker, 1999a). However, further studies revealed the role of carrier orientation and spatial frequency in responsiveness to second-order stimuli. Indeed, neurons responsive to second-order stimuli are also selective to orientation and spatial frequency of carrier (e.g. Mareschal and Baker, 1999b). Theses findings led to further investigations which constructed second-order stimuli using different combinations of carrier and envelope orientations and also to find a bigger number of responsive neurons to second-order stimuli (Li and Baker, 2012; Li et al., 2014). Although there is no fixed relationship between the optimal orientation of carrier and that of envelope (Mareschal and Baker, 1999a; Li et al., 2014), second-order responsive neurons have been shown to be well tuned to carrier orientations. The finding of carrier orientation tuning in second-order responsive neurons rules out any source of nonlinear artifact in those neuron responses (Zhou and Baker, 1993; Li et al., 2014) (Error! Reference source not found.). Indeed, those artifacts which might potentially arise from display device or photoreceptors, cannot yield such carrier tuning, or even if they can, it would be the same in every neuron. Therefore, the observed carrier tunings in previous studies that were variable among neurons and distinct from that of envelope, provided some evidence to exclude any contribution of artifacts in second-order responses.

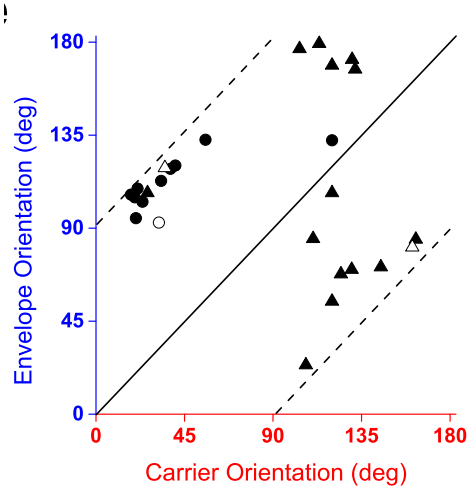

Figure 6. There is no fixed relationship between carrier (red) and envelope (blue) orientations. Other conventions as **Figure 5** (Adapted from Li et al., 2014).

Cortical organization of responsive neurons to second-order stimuli

The cortical organization of responsive neurons to second-order stimuli also has been investigated with imaging and electrophysiological methods (Zhan and Baker, 2006; Li and Baker, 2012). Intrinsic optical imaging in area 18 of cats revealed similar orientation preference maps for first-order and second-order stimuli. In fact, *LGs* and illusory and contrast envelopes evoked the same orientation preference maps in area 18. The orientation preference of neuronal populations in response to first- and second-order stimuli was very similar, such that a majority of neurons showed <30 degrees difference in orientation preference. However, the fraction of responsive neurons to second-order was less than that to first-order stimuli and neural responses to second-order were weaker than those to first-order stimuli. In addition, the population responses to contrast and illusory contours were immune to different carrier orientations and therefore second-order responses were dependent on envelope orientation rather than carrier. The similarities of first- and second-order maps led to the idea of homogeneous distribution of second-order neurons across the cortical surface (Zhan and Baker, 2006). However, conflicting with this notion, another study investigating the functional organization of responsive neurons to second-order stimuli, in area 18 cats, argued against the homogenous distribution of second-order neurons across the cortical surface and instead, showed that responsive neurons to second-order are highly clustered and organized in a columnar manner (Li and Baker, 2012). Indeed, nearby neurons shared similar spatial frequency and to some extent similar orientation preference of carrier, and moreover, they formed a columnar organization along the cortex. While both spatial frequency and orientation maps of carrier showed clustered organization, carrier orientation maps were more scattered and therefore, this mini-cluster organization could be missed in intrinsic optical imaging (Zhan and Baker, 2006), which accesses only the superficial layers and has limited spatial resolution (Li and Baker, 2012).

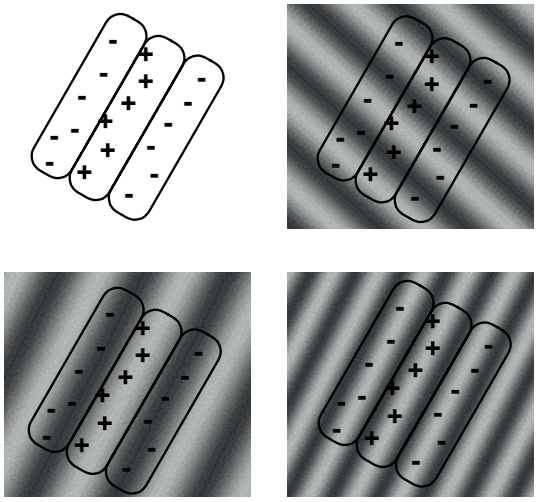

Figure 7. Luminance grating presented in an optimal spatial frequency and orientation evokes maximal neural responses (Adapted from Baker and Mareschal, 2001).

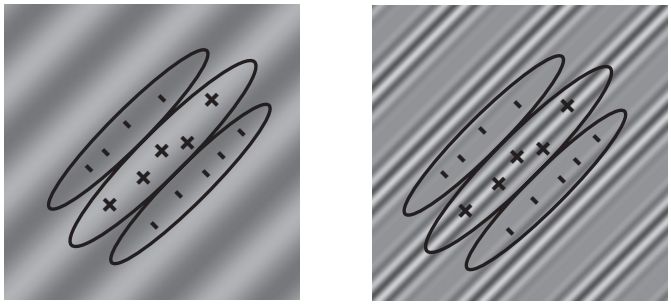

Figure 8. Linear mechanism cannot explain the second-order responses, unlike to first-order (Adapted from Baker and Mareschal, 2001).

Potential model for second-order processing

Filter-Rectify-Filter model

Linear summation is the well-known underlying mechanism of first-order stimuli to elicit a response in simple and complex cells. **Figure 7** illustrates how a conventional LG can activate simple cell sub-regions if it is presented with an optimal orientation and spatial frequency. As this figure shows, to evoke maximally effective summation, the orientation and spacing of dark and light bars have to be aligned with the excitatory and inhibitory sub-regions of the simple cell. Although complex cells do not show such spatially segregated excitatory and inhibitory sub-regions, they are selective to different orientations, spatial frequencies and velocities. Hubel and Wiesel in 1962 (Hubel and Wiesel, 1962) suggested that complex cells sum up the responses from neighboring simple cell type neurons, which have similar preferences, but slightly different receptive filed positions. Therefore, complex cells' orientation selectivity could be also explained by linear summation. However, a linear summation mechanism cannot account for second-order processing. As **Figure 8** shows while linear mechanism could account for luminance-modulated responses, *CG* responses could only be explained by a nonlinear mechanism. Although light and dark bars of an optimal LG can stimulate sufficiently the excitatory and inhibitory sub-regions of the receptive field of a simple cell and evoke a maximal response, the spatial frequency of the noise texture in *CGs* is too high to provide any net luminance changes within the neuron's receptive field. In fact, light and dark elements of the carrier cancel out within individual sub-regions of the receptive

field and thus linear summation cannot account for contrast-modulated responses. Although the underlying mechanism of second-order processing has been intensively debated (e.g. Tanaka and Ohzawa, 2009; El-Shamayleh and Movshon, 2011; Hallum and Movshon, 2014; Li et al., 2014), human psychophysics (Landy and Graham, 2004) and electrophysiological studies in higher-order mammals (Movshon et al., 1978b; Issa et al., 2000) suggested a two-stage model of second-order processing (Zhan and Baker, 2006). This model consists of two linear filters and one non-linear rectifier (**Figure 9**). According to this filter-rectify-filter (FRF) model, neurons with small receptive fields would respond to the carrier, and their output is rectified and summed by the second and larger linear filter of low spatial frequency, providing orientation-selectivity to the envelope. However, it is currently unclear which brain structures serve as filters, in particular the first-stage filter. Considering the established spatial frequency and orientation tuning of carrier, the potential candidate for the first stage has to be selective for those features. V1 neurons might be the primary potential candidates to play the first-stage filter role in filter-rectify-filter model, as they are selective for spatial frequency and orientation of carrier (Mareschal and Baker, 1999a). However, recent studies suggested that LGN neurons could provide carrier-tuned input for V1 neurons, as they are spatial frequency and orientation selective to carrier (Rosenberg et al., 2010; Rosenberg and Issa, 2011). In any manner, first-stage information will be carried by V1 neurons, which constitute the subunits of V2 receptive fields, and thus the complex images could be perceived by V2 neurons (Li et al., 2014).

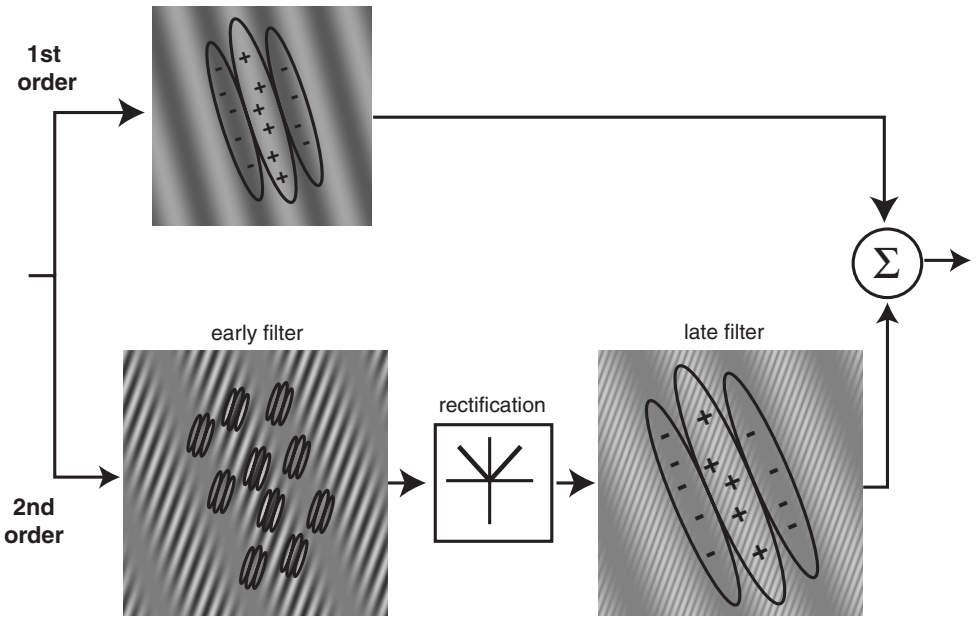

Figure 9. Two-stage model suggested for second-order processing (Adapted from Baker and Mareschal, 2001).

Surround suppression mechanism

Although several studies have postulated the filter-rectify-filter model as the underlying mechanism of second-order responses, it is uncertain if such a mechanism exists in primates and other mammals (e.g., Tanaka and Ohzawa, 2009; El-Shamayleh and Movshon, 2011; Hallum and Movshon, 2014; Li et al., 2014). Indeed, another series of second-order studies proposed that responses to second-order stimuli could arise from other mechanisms, such as surround suppression (Tanaka and Ohzawa, 2009; El-Shamayleh and Movshon, 2011; Hallum and Movshon, 2014). Tanaka and Ohzawa suggested that the spatial organization of center-surround of neurons in area 17 of cats

is suitable to encode the orientation of higher-order contours. Based of neural responses to second-order stimuli, they reconstructed the spatial organization of V1 classical receptive fields and their surrounds and found that center-surround receptive fields of V1 neurons, generally, are organized elongated and parallel to each other. These findings led them to conclude that center-surround receptive fields act as a spatial filter and extract the higher-order borders by their filter shapes (Tanaka and Ohzawa, 2009).

Mice as a popular model system for visual processing

Over the past few years, interest in mouse visual cortex has considerably grown. Until now, the non-human primate has been the preferred animal model for studies of cortical visual processing because it has an elaborate visual system whose key properties, such as acuity or color vision, are mostly similar to those of humans. In many other areas of neuroscience, however, mice have played a prominent role (Boulanger, 2009; Crook and Housman, 2011; Mentis et al., 2011), since the mouse is currently the only mammal in which genetic engineering methods are routinely employed. Here, the advent of transgenic and knockout techniques has provided abundant possibilities to study normal and abnormal brain function and its relationship to brain structure. Because the availability of such powerful methods holds the potential to resolve long-standing questions of cortical visual processing (Liu et al., 2009b) interest in the mouse model has grown in the field of visual systems neuroscience. In studies of cortical visual processing, the use of a system as simple as the mouse cortex, which lacks both fine-scale spatial acuity and columnar maps such as those for orientation, promises to determine minimal mechanisms necessary for receptive field development and function (Niell and Stryker, 2008b). Remarkably, recent studies show that some key response properties of mouse visual neurons are actually quite comparable to those known from decades of study in higher mammals (Niell and Stryker, 2008b; Gao et al., 2010b; Van den Bergh et al., 2010). These properties include the sharp tuning for orientation, luminance-invariant contrast sensitivity and contrast-dependent temporal and spatial frequency sensitivity.

Functional organization of mouse higher visual areas

Although the mouse visual cortex is much more simple in both structure and function compared to primates and higher mammals, it still shares some basic similarities (Niell and Stryker, 2008a; Gao et al., 2010a; Van den Bergh et al., 2010) For example, anatomical studies have established around 10 separated, retinotopically organized areas in mouse visual cortex (**Figure 10**). These areas include the primary visual area, which is surrounded by nine other extrastriate areas, each containing a complete map of the entire visual hemifield (Wang et al., 2007b). Despite the ongoing debate on the functional division of rodent extrastriate areas, studies based on cytoarchitectonic and chemoarchitectonic markers and pathway tracing have categorized these areas into two parallel streams: the ventral stream which consists of LM, LI, POR, P and which is suggested to be responsible for object recognition; and the dorsal stream which consists of AL, PM, AM, A, RL and is proposed to be involved in object localization (Wang et al., 2011, Wang et al., 2012). Furthermore, distinct mouse extrastriate areas have been shown to have, to some extent, functional differences as well, when they are probed with first-order gratings (Van den Bergh et al., 2010; Andermann et al., 2011; Marshel et

al., 2011; Glickfeld et al., 2013). For example, neurons in area AL, the gateway to the dorsal stream, prefers visual stimuli with higher temporal frequency and lower spatial frequency and therefore might be involved in object localization, while neurons in PM are driven better by high spatial frequency and low temporal frequency gratings and thus might have a role in detecting fine texture (Andermann et al., 2011; Marshel et al., 2011). Therefore, both anatomical and functional studies support the idea of existence of ventral and dorsal streams in mouse visual cortex, similar to those in higher mammals, but probably in a basic and simple manner.

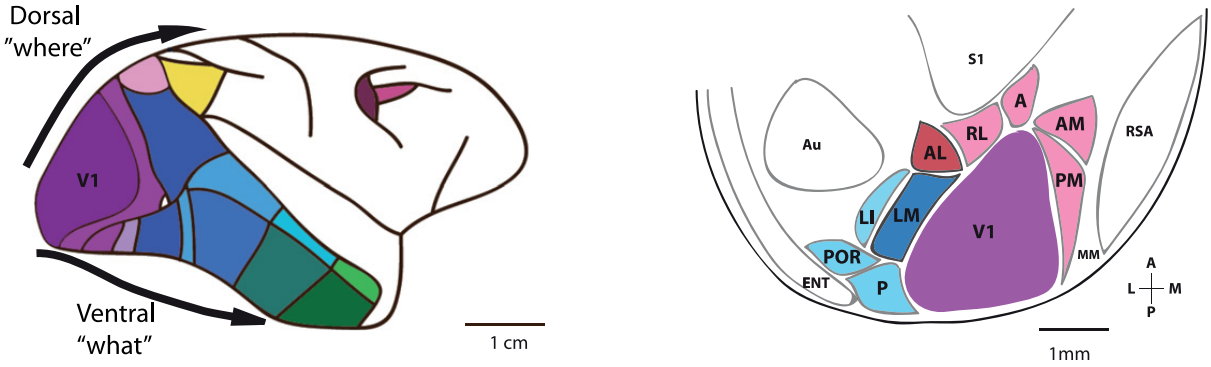

Figure 10. Extrastriate visual areas in the primate and mouse (Adapted from Niell, 2011)

Can mice vision rely on more than luminance cues?

Although the number of studies exploring mouse vision has been growing in recent years, it is still not clear whether and how mice can extract meaningful representations from visual cues other than luminance. Studies comparing the basic properties of mouse visual areas (Van den Bergh et al., 2010; Andermann et al., 2011; Marshel et al., 2011) and examining the functional specificity of cortico-cortical projections (Glickfeld et al., 2013) used only first-order, *LGs*. Although using *LGs* offers several advantages such as direct comparison of the properties of extrastriate and V1 neurons and precise measurements of basic and discriminating features of ventral and dorsal streams (i.e. spatial frequency and temporal frequency), they may not drive higher-order neurons optimally. Also, in psychophysical studies where mice had to perform visual tasks (Andermann et al., 2010; Histed et al., 2012; Lee et al., 2012; Bennett et al., 2013), so far, only *LGs* have been employed. Therefore, it is not established yet whether and how the mouse visual system represents other visual cues than luminance and if mice can use those second-order stimuli to guide visual behavior.

Area LM might be a suitable area to investigate second-order processing

Among mouse extrastriate areas, LM has been thought to be homologous to area V2 in higher-order mammals, where selectivity for second-order contours has been found (Zhou and Baker, 1994; Leventhal et al., 1998; Mareschal and Baker, 1998a, b; Zhan and Baker, 2006; Song and Baker, 2007; Li et al., 2014). V2 and area LM are similar in several aspects: both areas share the representation of the vertical meridian with V1 (Coogan and Burkhalter, 1993); Wang et al., 2007b), both areas are primary targets of V1 projections (Wang et al., 2011) and both contains neurons with ventral and dorsal

stream properties (Wang et al., 2012). Another reason that makes LM a suitable area to study second-order processing in mouse is the potential role of this area in object recognition, as anatomical studies identified area LM as the gateway of the mouse ventral stream (Wang et al., 2011). Furthermore, one study in rodents showed that LM lesions could disrupt some aspects of object recognition (Sacco and Sacchetti, 2010). Taken together, the established properties of area LM make this area as an interesting, putative region involved in second-order processing.

Can mice use second-order stimuli to guide visual perception in a cue-invariant way?

In this study I investigated whether mice can use second-order stimuli to guide visual perception in a cue-invariant way and examined potential cue-invariant representations of stimulus orientation in two areas of mouse visual cortex. Using a classical condition task, I tested whether orientation discrimination could be achieved invariant to defining cue of visual stimuli. More precisely, I asked if mice can generalize orientation discrimination from first-order *LGs* to second-order, *CGs*. I found that mice are capable of generalizing orientation discrimination learning from familiar cue conditions to novel cue conditions. Then I performed extracellular recordings of neural responses to LG and CG stimuli in mouse areas V1 and LM, and compared the orientation tuning curves to these two types of gratings. Although in both areas the responses to *CGs* compared to those to *LGs* were weaker and less selective, neurons showed broadly similar preferences for the two types of stimuli. I conclude that mice are able to use second-order stimuli to guide visual perception, albeit in a basic form.

Material & Methods

All procedures complied with the European Communities Council Directive 2010/63/EC and the German Law for Protection of Animals, and were approved by local authorities, following appropriate ethics review.

Luminance-modulated and contrast-modulated gratings

Visual stimuli were presented using custom software (EXPO; https://sites.google.com/a/nyu.edu/expo/home) on a calibrated liquid crystal display (LCD) monitor (Samsung 2233RZ; mean luminance 50 cd/m^2), placed 25 cm in front of the animal's eyes. To correct luminance nonlinearities of the display I used an inverse gamma lookup table obtained regularly by calibration with a photometer.

For both behavioral and electrophysiological experiments, I used a common set of luminance-modulated gratings *(LGs)* and contrast-modulated gratings *(CGs)*, obtained by multiplying a contrast envelope with a noise carrier. I defined a two-dimensional moving sine wave grating as: $S(x, y, t) = \sin(2\pi f(\sin(\theta)\, x + \cos(\theta)\, y) + 2\pi v t)$, where f is the spatial frequency, θ is the orientation, and v is the temporal frequency. *LGs* were then generated as: $LG(x, y, t) = l_0 + l_0 c S(x, y, t)$, and *CGs* were generated as $CG(x, y, t) = l_0 + l_0(S(x, y, t) + 1)/2 * N(x, y)$, where $l_o$is the mean luminance, c is the contrast and $N(x, y)$ is the static noise carrier with a spatial frequency spectrum that dropped off as $A(f_n) \sim 1/(f_n + f_c)$. I created two types of *CG* stimuli that differed in the distribution of Fourier energy of the carrier. For *CGs* with low-frequency noise, I set f_c to 0.05 cycles/degree and imposed a high frequency cutoff at 0.12 cycles/degree; for *CGs* with high frequency noise, I used an $f_c = 0$ cycles/degree and a low frequency cutoff at 0.12 cycles/degree. For recordings from area V1, the *LGs* and the envelope of the *CGs* had a spatial frequency f of 0.05 cycles/degree and a temporal frequency v of 1.5 Hz. To optimize stimulus parameters for the preferences of area LM, I conducted the LM recordings with f of 0.028 cycles/degree and v of 1.8 Hz (Marshel et al., 2011). Contrast c was set to 1, except for experiments where I matched the root-mean-square (RMS) contrast between first- and second-order gratings, in which case c was 0.335 for the *LGs*. The seed for generating the random Gaussian noise texture was varied across experimental sessions.

Analysis of visual stimuli

Following An et al. (2014), I performed a spectral power analysis of the *LGs* and *CGs*. To reveal the difference in power between two orthogonal orientations, I first calculated $D(\omega_x, \omega_y, \tau) = P_{\mathrm{o}}(\omega_x, \omega_y, \tau) - P_{\mathrm{o\_ortho}}(\omega_x, \omega_y, \tau)$, where the power P is the squared amplitude of the 3-dimensional Fourier transform of the drifting grating. To illustrate the difference in power as a function of space, D was further integrated to result in $I(\omega_x, \omega_y) = \int D(\omega_x, \omega_y, \tau) d\tau$. To illustrate the difference in power as a function of orientation, $I(\omega_x, \omega_y)$ was transformed into $\tilde{I}(\rho, \theta)$ and was further integrated to result in $O(\theta) = \int \tilde{I}(\rho, \theta) d\rho$. To assess the spatial frequency and temporal frequency content of the absolute differential power, I calculated $S(\rho) = \int \left|\tilde{I}(\rho, \theta)\right| d\rho$ and $T(\tau) = \iint \left|P_{\mathrm{o}}(\omega_x, \omega_y, \tau) - P_{\mathrm{o\_ortho}}(\omega_x, \omega_y, \tau)\right| d\omega_x d\omega_y$.

Surgical preparation for head-fixed visual behavior

Behavioral experiments were performed in 2-5 months old C57BL/6J mice of either sex (2 males, 4 females). General anesthesia was induced by 5% isoflurane and maintained during surgery at 1–2%. Buprenorphine (0.1 mg/kg, sc) was used for analgesia and atropine (0.3 mg/g, sc) to reduce bronchial secretions. Animal temperature was kept at 37°C. A custom-designed head post was mounted to the skull using dental cement (Tetrik EvoFlow, Ivoclar Vivadent). Mice were implanted with two miniature screws over the cerebellum (#00-96X 1/16, Bilaney), serving as reference and ground with extracellular recordings. The skull over the target area was marked and sealed with KwikKast (WPI). For 3 days after surgery, mice were injected by antibiotics (Baytril, 5mg/kg, sc) and longer lasting analgesics (Carprofen, 5mg/kg, sc). After recovery, mice were gradually habituated to being head-fixed and placed on an air-suspended Styrofoam ball (Holscher et al., 2005; Dombeck et al., 2007) (**Figure 1***a*). A spout connected to a lick sensor was used to measure licks and deliver fluid rewards (Schwarz et al., 2010).

Orientation discrimination task and analysis of behavioral data

After habituation to the setup, mice were placed on a water restriction regimen. Throughout all training phases, the animals' daily weight and fluid consumption were monitored and recorded, and the animals were checked for signs of potential dehydration (Guo et al., 2014). Following Guo et al. (2014), in a first phase, daily access to water was systematically reduced until the animal reached a target weight of ~85% of its initial weight. After the weight had stabilized, training in the behavioral task started and mice received most of their water during performance in the behavioral apparatus.

Using classical conditioning, mice were trained to associate the orientation of the visual stimulus with a water reward. In each session, mice were presented with 120 trials of either 45 deg or 315 deg gratings, drifting for a duration of 3 s behind an aperture of 32 deg diameter. The presentation of the 315 deg grating was automatically followed by a fluid reward of 5-7 µl , the orthogonal grating was never rewarded. Stimulus presentations were separated by an interstimulus interval of 15 s added to a random delay drawn from an exponential distribution with a mean of 15 s. Drawing onset times from an exponential distributions yields a flat hazard rate, ensuring that animals cannot predict the time point of reward delivery.

To evaluate orientation discrimination performance, I focused on licks in anticipation of fluid reward. Following Gallistel et al. (2004), I computed, separately for each stimulus orientation, a lick index $LI = (licks_{stimulus} - licks_{baseline})/(licks_{stimulus} + licks_{baseline})$, where $licks_{stimulus}$ is the number of licks during the last 1 second of stimulus presentation and $licks_{baseline}$ is the number of licks during the 1 second before stimulus presentation. To identify learning I analyzed the cumulative records of *LI*, where changes in slope correspond to changes in the level of performance. For instance, a positive slope of the cumulative *LI* corresponds to increased licking during the stimulus compared to the baseline period, and indicates that the animal anticipates reward after seeing any of the stimuli. A positive slope of the difference between cumulative *LIs* indicates that the animal licks more strongly during the rewarded than during the unrewarded grating, and shows that the animal has learned to discriminate grating orientations. To assign trials to different stages of orientation discrimination learning, I determined significant

changes in the slope of the difference of the cumulative *LI* by using a change point analysis (Gallistel et al., 2001). To quantify discrimination performance across the different stages of learning, I performed an ideal observer analysis on the distributions of *LI*s for the two orientations.

I tested the mice in several conditions. I always started training using *LGs* until the animal reached stable and reliable orientation discrimination performance. Then, I replaced *LGs* with *CGs* with low-frequency noise carriers to test the generalization of orientation discrimination to second-order gratings. To test for influences of stimulus contrast, I switched back to *LGs*, but with contrast reduced to 0.335, such that it matched the RMS contrast of *CGs*. After that, 2 animals were additionally tested with *CGs* with high-frequency noise carriers.

Surgical preparation for electrophysiological recordings during wakefulness

Electrophysiological recordings were performed in 2-5 months old C57BL/6J mice of either sex (4 males, 8 females). Surgical procedures were identical to those for behavioral experiments. After recovery and habituation to the setup, mice underwent a second surgical procedure under general anesthesia (1-2% Isoflurane, ~15 min), in which a craniotomy was performed, which was sealed with KwikKast until the recording session. To avoid potential effects of anesthesia, recordings were never performed on the same day of the craniotomy.

Surgical preparation for electrophysiological recordings during anesthesia

For electrophysiological recordings under anesthesia, I used 4 C57BL/6J mice. Anesthesia was induced by 5% isoflurane and maintained during surgery by a combination of urethane (375 mg/kg, ip), chlorprothixene hydrochloride (2 mg/kg, ip) and isoflurane (1–2%). I used Buprenorphine (0.1 mg/kg, sc) analgesia and atropine (0.3 mg/g, sc) to reduce bronchial secretions. Animal temperature was kept at 37°C. A custom-designed head post was mounted to the skull using dental cement (Tetrik EvoFlow, Ivoclar Vivadent). As reference, I used a wire placed into the cerebellum; as ground, a wire placed under the exposed skin. During recordings, isoflurane was kept at minimal to reduce unwanted side effects on visual responses (Vaiceliunaite et al., 2013). Depending on the level of anesthesia as assessed by the breathing rate and presence or absence of the pinch toe reflex, additional doses of chlorprothixene hydrochloride (2mg/kg, ip) were injected (approximately every 3 h). Recordings typically lasted for 6 h.

Recordings from V1 were obtained through a craniotomy (<1.5 mm) located 3 mm lateral to the midline and 1.1 mm in front of the anterior margin of the transverse sinus. Recordings from LM were obtained from 4 mm lateral to the midline and 1.4 mm in front of the anterior margin of the transverse sinus “Wang, 2011”. Recordings from V1 and LM were performed in separate sessions using 32-channel silicon probes in a 4-shank configuration (Buzsaki32-A32, Neuronexus; 200 inter-shank spacing). Extracellular signals were recorded at 30 kHz (Blackrock microsystems). Online estimates of tuning properties relied on high-pass filtered signals crossing a fixed threshold (typically 4.5–6.5 SDs).

Visual stimuli for electrophysiological recordings

To estimate receptive field (RF) position, I mapped ON and OFF subfields of RFs using a sparse noise stimulus (Liu et al., 2009a). This stimulus consisted of white or black squares (4° diameter) briefly flashed (150 or 200 ms) on a square grid (40 or 60° diameter). Subsequent stimuli were centered on the online estimates of the average RF maps for each shank of a 32-channel silicon probe (see "Analysis of electrophysiological data" and **Figure 1***b*). To measure orientation tuning curves, I interleaved in pseudo-random order *LGs* and *CGs* moving for a duration of 2 s in 8 different directions.

Analysis of electrophysiological data

Unit extraction and spike sorting

Recordings from V1 were obtained through a craniotomy (~1.5 x 1.5 mm) located 3 mm lateral to the midline and 1.1 mm in front of the anterior margin of the transverse sinus. Recordings from LM were obtained from 4 mm lateral to the midline and 1.4 mm in front of the anterior margin of the transverse sinus (Wang et al., 2011). Recordings from V1 and LM were performed in separate sessions using 32-channel silicon probes in a 4-shank configuration (Buzsaki32-A32, Neuronexus; 200 µm inter-shank spacing, **Figure 1***b*). Extracellular signals were recorded at 30 kHz (Blackrock microsystems). Online estimates of tuning properties relied on high-pass filtered signals crossing a fixed threshold (typically 4.5–6.5 SDs).

Wideband extracellular signals were digitized at 30 kHz (Blackrock microsystems) and analyzed using the NDManager software suite (Hazan et al., 2006). The 8 channels on each shank were treated as an "octrode". Using a robust spike detection threshold (Quiroga et al., 2004) set to 6 standard deviations of the background noise, spike-waves were extracted for each "octrode" from the high-pass filtered continuous signal. The first 3 principal components of each channel were used for automatic clustering with KlustaKwik, followed by manual refinement of clusters (Hazan et al., 2006). This yielded high-quality single unit activity as evident from distinct spike wave shapes and a clear refractory period in the autocorrelogram (**Figure 1***d*). For analysis of retinotopy, I used the envelope of the multiunit activity (MUAe, van der Togt et al., 2005), averaged across all channels in each shank.

Analysis of tuning

To determine RF maps for single unit spiking activity, I fitted ON and OFF subfields separately with a two-dimensional Gaussian (Liu et al., 2009a): $f(x,y) = B + \frac{A}{2\pi ab}\exp\left(-\frac{x'^2}{2a^2} - \frac{y'^2}{2b^2}\right)$, where A is the maximum amplitude, B is the baseline response, a and b are half-axes of the ellipse, and x' and y' are transformations of the stimulus coordinates x and y, taking into account the angle θ and the coordinates of the center (xc, yc) of the ellipse. To quantify the progression of RF location in the recorded visual area, I constructed maps of z-scored MUAe activity, averaged between 0 – 0.35 s after stimulus onset. If these maps had a sufficient signal/noise ratio (standard deviation > 0.035), I computed the average RF coordinates from the peak of the MUAe activity for each shank. Sessions with ambiguous maps were discarded from all further analyses.

Orientation tuning curves were fitted with a sum of two Gaussians with peaks 180 deg apart, which could have different amplitudes but equal width and a constant baseline. To quantify orientation selectivity, I computed d-prime (Berens et al., 2008) defined as

$d' = \frac{(\mu_{\text{pref}} - \mu_{\text{ortho}})}{\hat{\sigma}}$, where $\hat{\sigma} = \sqrt{(\sigma^2_{\text{pref}} + \sigma^2_{\text{ortho}})/2}$. In contrast to the more commonly used OSI (Niell and Stryker, 2008a), this index has the advantage to not only consider modulation depth but also the variability of responses. I performed all our analyses also on OSI (both with and without spontaneous activity removed), and circular variance (Ringach et al., 2002); results obtained with these alternative measures were qualitatively similar. I only considered neurons which passed 3 selection criteria applied to the responses to *LGs*: (1) an average firing rate of at least 1 spike/s to at least one orientation, (2) average responses to at least 2 orientations differing from the response to the mean-luminance gray screen by at least 2.58 times the standard error of the mean, and (3) explained variance of the Gaussian fit of at least 70%.

Comparison of responses to luminance-modulated and contrast-modulated gratings

On the population of selected neurons, I performed a log-linear analysis to statistically assess the proportion of neurons responsive to both *LGs* and *CGs* vs. *LGs* only. To model the observed counts, I fitted a generalized linear model (GLM) with a Poisson link function considering the factors responsiveness (*LGs and CGs* vs. *LGs only*) and area (V1 vs. LM). I report all significant interactions with the factor responsiveness. In addition, I included the factor noise (low-frequency vs. high-frequency) to assess differences in responsiveness across experiments with different noise textures.

To investigate differences in firing rates and orientation tuning in response to *LGs* and *CGs* I performed an analysis of variance (ANOVA) with the within-subject factor stimulus (*LGs* vs. *CGs*), and the between-subject factors area (V1 vs. LM). To appropriately visualize the results, I show the mean and standard error of the pairwise differences (Franz and Loftus, 2012). To compare the difference in responses to *CGs* vs. *LGs,* for *LGs* with full contrast and matched RMS contrast, I performed an ANOVA with the within-subject factor stimulus (*LGs* vs. *CGs*), and the between-subject factors contrast (full vs. matched *LG*) and area (V1 vs. LM). All post-hoc pairwise contrasts were corrected for multiple comparisons (multcomp package in R, (R Development Core Team, 2015).

To relate the preferred orientations in response to *LGs* and *CGs* I used the circular version of the Pearson's product moment correlation as described by (Jammalamadaka and Sengupta, 2001) and implemented in Matlab by (Berens, 2009).

Histology

For post-mortem histological reconstruction of recording sites (**Figure 1***c*) I coated each shank of the electrode alternating between a red-shifted fluorescent lipophilic tracer (DiD; D7757, Invitrogen) and an orange fluorescent lipophilic dye (DiI; D282, Invitrogen). After recordings, mice were transcardially perfused under pentobarbital sodium anesthesia (200 mg/kg) with 0.2 M sodium phosphate buffer (PBS), followed by 4% paraformaldehyde in PBS. Brains were postfixed for 24 h at 4°C and then rinsed 3 times with 1x PBS. Brains were sliced (40 µm) using a vibratome (Microm HM 650 V-Thermo Scientific) and mounted on glass slides with Vectashield DAPI (Vector Laboratories), and coverslipped. Slides were inspected for the presence of the tracers using a Zeiss Imager.Z1m fluorescent microscope.

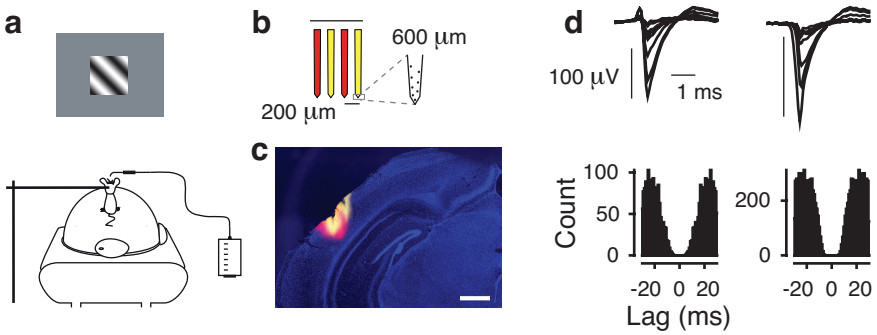

Figure 1. Behavior setup, recordings, and isolated single neurons. ***a***, Setup for head-fixed behavior with air-cushioned spherical treadmill and lick-sensor. ***b***, Schematic of the four-shank silicon probe. ***c***, Coronal section. The four shanks of the electrode were stained in alternating fashion with DiI (yellow) and DiD (red). Blue represents DAPI. Scale bar, 400 m. ***d***, Average spike-waveforms and autocorrelograms of two example single units recorded from area V1. Units 144 –5.x.31 and 144 – 4.x.5.

Results

Stimuli

To discriminate the global, first-order and local, second-order features of *CGs*, I performed a spectral analysis of the stimuli used in this study. **Figure 1** shows the spectral analysis performed on the grating orientations used for the behavioral experiments. *LGs* (**Figure 1***a*$_1$) contain power at a single spatial frequency and orientation (**Figure 1** *a*$_2$) and the peaks of their differential power in the orientation domain correspond to grating orientations, i.e. at −45 and 45 degrees (**Figure 1***a*$_3$, *a*$_4$). The absolute differential power in the spatial frequency domain peaks at 0.05 cycles/degree (**Figure 1***a*$_5$) and the absolute differential power in the temporal frequency domain peaks at 1.5 Hz (**Figure 1***a*$_6$), which correspond to the grating spatial frequency and temporal frequency, respectively. For *CGs* with low-frequency noise carrier (**Figure 1***b*$_1$, *b*$_2$), the differential power peaks at −45 and 45 degrees, which correspond to the orientation of envelope (**Figure 1***b*$_3$, *b*$_4$). This is due to an inhomogeneity in the distribution of local luminance of the noise carrier, induced by the envelope. However, the magnitude of this differential power is considerably different from that for *LGs*, it is smaller (25% of that for *LGs*) and more broadly distributed across orientations. In the spatial frequency domain also, *CGs* with low-frequency noise show a broad differential power distribution between 0.02 and 0.15 cycles/degree (**Figure 1***b*$_5$), while in the temporal frequency domain, absolute differential power peaks clearly at 1.5 HZ, corresponding to the drift rate of the envelope (**Figure 1***b*$_6$). In comparison, the spectral analysis on *CGs* with high-frequency noise carrier (**Figure 1***c*$_1$, *c*$_2$) revealed only little differential power across spatial frequencies (**Figure 1***c*$_3$), as no clear peaks and troughs of differential power were observed around the orientations of the *LGs* (**Figure 1***c*$_4$). For this type of *CGs*, the absolute differential power in the spatial frequency domain is small for values lower than 0.08 cycles/degree, highest at 0.16 cycles/degree, and diminishes toward higher spatial frequencies (**Figure 1***c*$_5$); the absolute differential power in the temporal frequency domain again peaks at 1.5 HZ, which is the drift rate of the envelope (**Figure 1***c*$_6$).

Together, this spectral analysis reveals the difference between the two types of *CGs* in activating the first-order luminance-sensitive mechanism in the mouse visual system: while the distortion signals in *CGs* with low-frequency noise carriers could lead to decoding stimulus orientation via first-order mechanisms, it seems unlikely that *CGs* with high-frequency noise carrier invoke the same mechanism. Indeed, as explained above, for *CGs* with high-frequency noise carrier, there are no clear peaks and troughs around the orientation of the *LGs* in the differential orientation signal across spatial frequencies and the spatial frequencies of the noise carrier are concentrated beyond the optimal values for mouse V1 (0.045 cycles/degree) and LM (0.028 cycles/degree) neurons (Marshel et al., 2011).

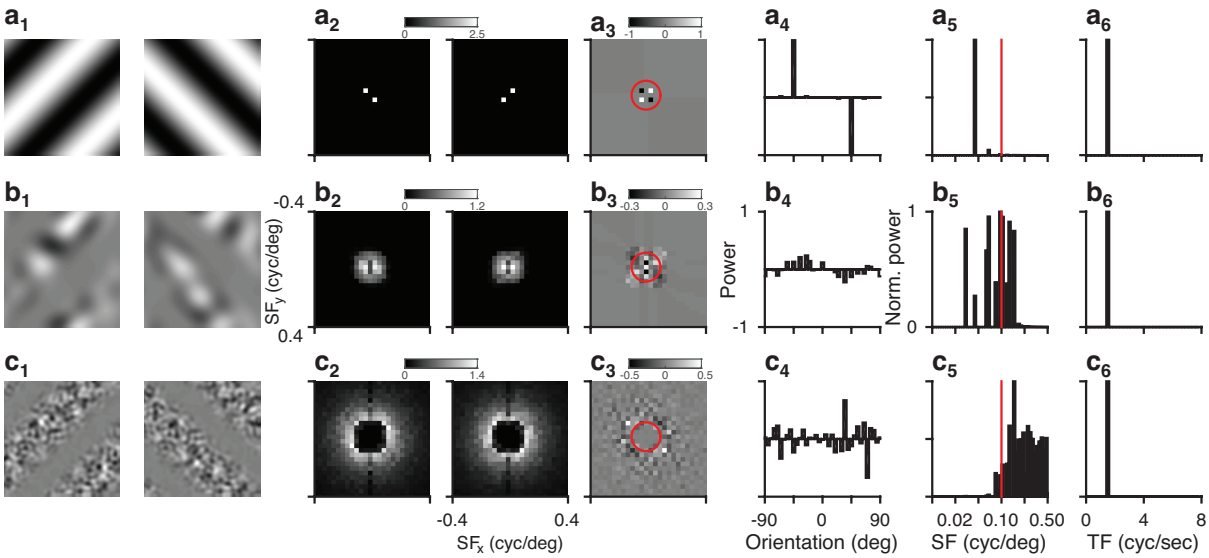

Figure 1. Analysis of visual stimuli. ***a***, *LGs* (32 degrees wide) of orthogonal orientations (a_1) and their power spectra (a_2). Differential power in the Fourier plane (a_3) and orientation domain (a_4). Spatial frequency (a_5) and temporal frequency content (a_6) of the absolute differential power distribution. ***b***, Same as *a*, for the *CGs* with low-frequency noise. ***c***, Same as *a*, for the *CGs* with high-frequency noise. Red circles and lines indicate a spatial frequency of 0.1 cycles/degree.

Orientation discrimination learning for luminance-modulated gratings

I wanted to test whether mice can use second-order stimuli to guide visual perception in a cue-invariant way. In order to address this question, first I trained head-fixed mice in a classical conditioning paradigm to discriminate different orientations of *LGs* (**Figure 2**). I presented two orthogonal orientations and paired one of these orientations with a fluid reward. Next, I measured discrimination performance with analyzing the orientation-specific licking in anticipation of reward. At the beginning of training, animals licked constantly, regardless of stimulus presentation and increased lick rates to pick up the reward (**Figure 2**a). However, when animals learned the task, a high rate of licks was observed during the presentation of the rewarded orientation (**Figure 2**b). To evaluate licking, I computed, for each orientation separately, the cumulative sum of a lick index (*LI*), defined as the difference in the number of licks during the last 1 s of stimulus presentation and the 1 s before stimulus presentation, divided by their sum (**Figure 2**c). Then, I calculated the difference between cumulative *LIs* to the rewarded and unrewarded orientations and identified significant change points, which are related to significant changes in orientation discrimination performance (**Figure 2**d). Later, I performed an ideal observer analysis on the animal's *LI*, which indicated that orientations could not be decoded before (area under the receiver operating characteristic [AUROC] = 0.52, 95% CI = 0.50– 0.55), but after learning (AUROC = 0.78, 95% CI = 0.75– 0.80). Finally, I summarized the performance across all mice and found similar results, with average performance increasing from 0.51± 0.008 (SEM) to 0.80 ±0.023.

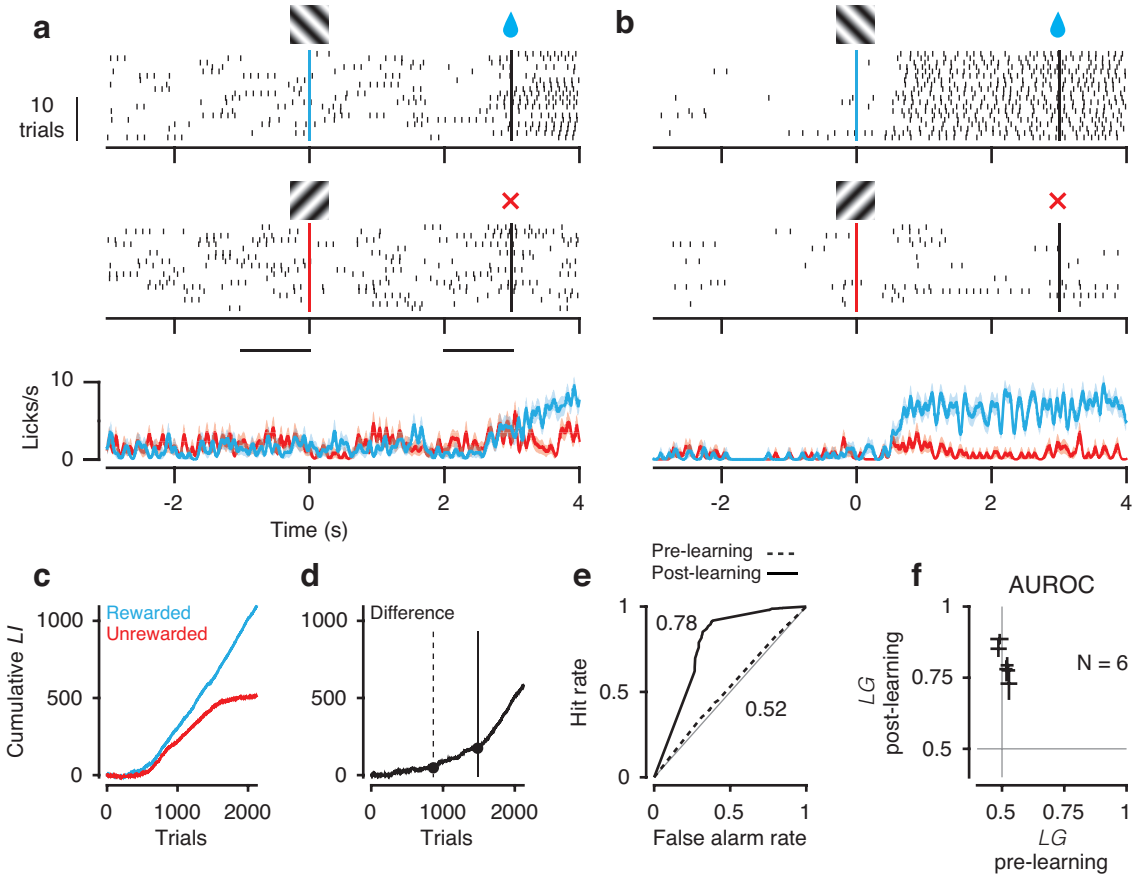

Figure 2. Orientation discrimination for *LGs*. ***a***, Example behavioral session, before learning. Top, Licks to the rewarded orientation. Middle, Licks to the unrewarded orientation. Bottom, Trial-averaged lick density. Shaded regions represent mean SEM. Gratings indicate stimulus onset. Black vertical lines indicate stimulus offset. Black horizontal lines indicate baseline and stimulus period used for computing the *LI*. Session 5, ***b***, Same as ***a***, after learning. Session 21, ***c***, Cumulative *LI* as a function of trial number for rewarded (blue) and unrewarded orientations (red). ***d***, Difference of cumulative *LIs* between the two orientations. Dots indicate significant change points used for assigning sessions to training stages. Trials before the first change point were assigned to the pre-learning stage (dashed vertical line). Trials after the last change point (solid vertical line) were assigned to the post-learning stage. ***e***, ROC analysis based on distributions of *LIs* from the two conditions in the pre-learning stage (dashed curve) and post-learning stage (solid curve). ***a–e***, Example mouse 278. ***f***, AUROC across mice (N= 6). Crosses represent 95% CIs.

Cue-invariant generalization of orientation discrimination

Next, I tested whether mice can generalize the learned orientation discrimination from *LGs* to *CGs*, in which orientation was characterized by changes in contrast rather than luminance (**Figure 1***b*). After mice had successfully learned the orientation discrimination task and reached a stable and reliable performance, I switched only the stimulus from *LGs* to *CGs* and kept all other aspects of the task identical. I replaced *LGs*, first, with low-frequency noise carriers *CGs* because this would help to transfer of learning easier. Although the global appearances of *LGs* and *CGs* with low-frequency noise carrier are different, mice could, in principle, discriminate the two orientations of the low-frequency *CGs* by relying on first-order mechanisms similar to those optimal for the learned task with *LGs*. The positive slopes of the cumulative *LIs* for rewarded and unrewarded stimuli indicate that mice could distinguish the *CGs* from the mean-luminance gray background. I also found that all tested animals, with the exception of one mouse, could judge the orientations of *CGs* with low-frequency noise carrier, as evident from the steeper increase of *LI* for the rewarded compared with the unrewarded condition (**Figure 3***a*). Furthermore, no significant changes were found in

the slope of the differential cumulative *LI* across trials, which means mice did not need to learn the orientation discrimination task from scratch but instead could readily generalize from *LGs* to *CGs* (**Figure 3***b*). The fact that the slope of the differential cumulative *LI* does not significantly change across trials also indicates that even extensive training of almost 2000 trials did not improve the performance for *CGs*. Overall, mice showed a considerably lower performance for *CGs* with low-frequency noise (AUROC = 0.63, 95% CI = 0.62–0.65; **Figure 3***c*) than for the *LGs* and all tested mice showed the similar results (mean AUROC = 0.58 ± 0.017 SEM; **Figure 3***d*).

I wondered whether the lower RMS contrast of *CGs* compared with *LGs* could account for the overall lower performance for *CGs*. To test this hypothesis, I performed control experiments in which the RMS contrast of *LGs* was lowered to match that of *CGs* and trained mice with these RMS contrast matched *LGs* in the next phase. Mice showed a good performance during the orientation discrimination task for *LGs* matched in RMS contrast (mean AUROC = 0.83 ± 0.03 SEM; **Figure 3***e*–*g*). Indeed, summarizing the performances across all tested mice revealed similar results for both levels of contrast (p = 0.23, paired t test; **Figure 3***h*).

Finally, I probed mice with the other type of *CGs*, for which I imposed a low-frequency cutoff on the noise carrier. This type of *CGs* did not contain any energy at the spatial frequency of the learned *LGs* and little differential power across spatial frequencies at the learned orientations (**Figure 1***c*). Again, mice could distinguish *CGs* with high-frequency noise carrier from the mean-luminance gray background, evident in the positive slope of cumulative *LIs* across trials (**Figure 3***i*). Importantly, the mouse could also tell the two grating orientations apart, which is revealed by the increase in the difference of cumulative *LIs* (**Figure 3***j*); however, its performance for this type of *CG* was again considerably lower compared with that for *LGs* (AUROC = 0.58, 95% CI = 0.56 – 0.60; **Figure 3***k*). Similar results were obtained when I tested a second mouse (AUROC = 0.56, 95% = CI 0.53– 0.60; **Figure 3***l*). Together, these results reveal the ability of mice in using second-order stimuli to guide visual perception.

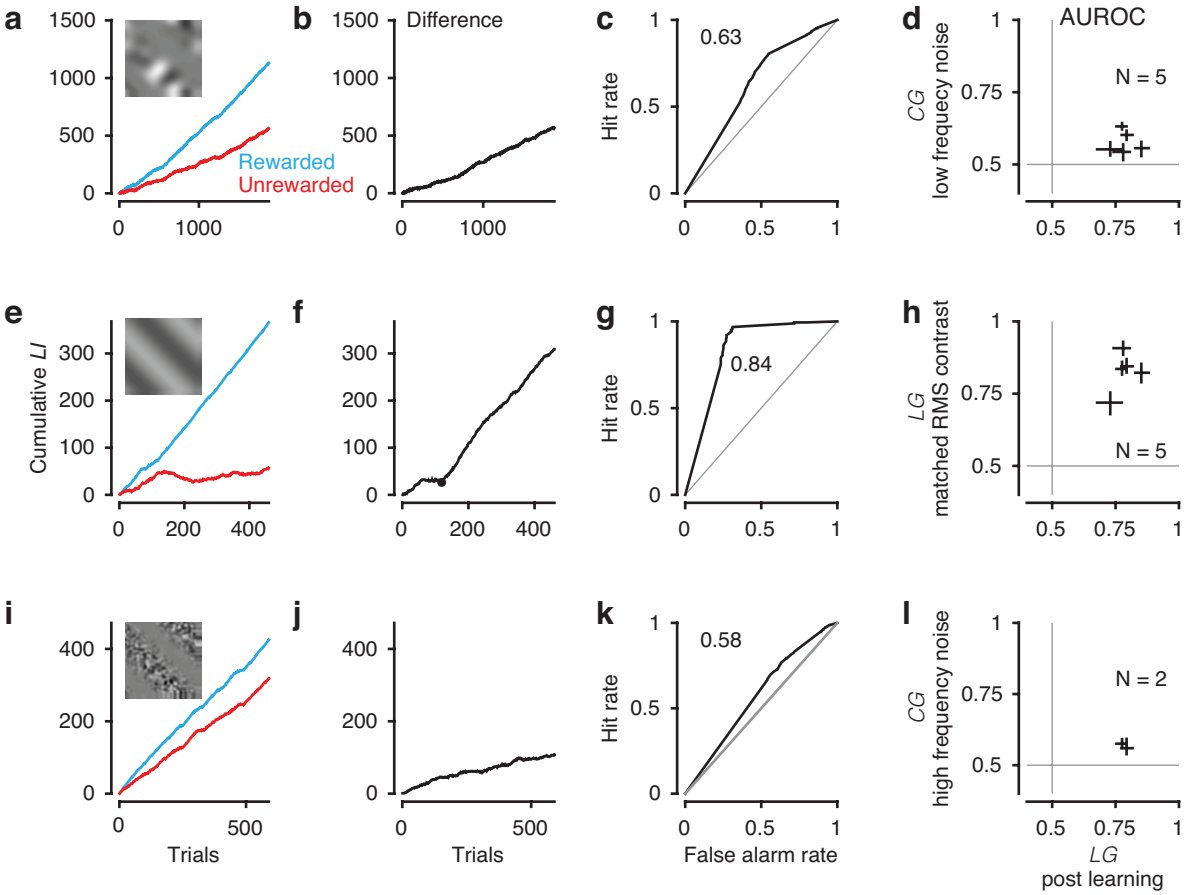

Figure 3. Behavioral performance for *CGs* and control conditions. ***a–d***, Performance for *CGs* with low-frequency noise carrier. ***a***, Cumulative *LI* as a function of trial number. Blue represents rewarded orientation. Red represents unrewarded orientation. ***b***, Difference of cumulative *LI* between the two orientations. ***c***, ROC analysis based on *LIs*. ***a–c***, Example mouse 278. ***d***, Comparison of AUROC values for *LGs* (after learning; Fig. 3f) and *CGs* ($N = 5$ mice). Crosses represent 95% CI. ***e–h***, Same as ***a–d***, for performance for *LGs* matched in RMS contrast. ***g***, I only considered data with stable performance (i.e., trials after the first change point in *f*). ***i–l***, Same as ***a–d***, for performance for *CGs* with high-frequency noise carrier ($N = 2$ mice). Conventions as in **Figure 2**.

Identification of areas V1 and LM based on mirrored retinotopic representation of azimuth

To investigate potential neural correlates of observed cue-invariant generalization of orientation discrimination in behavioral experiments, I performed extracellular recordings from areas V1 and LM. It has been established that area LM in mouse shares the vertical meridian with V1 (Coogan and Burkhalter, 1993; Wang and Burkhalter, 2007) and therefore is thought to be homologous to area V2 in higher-order mammals, where neurons have been indicated to be selective for second-order contours (Zhou and Baker, 1994; Leventhal et al., 1998; Mareschal and Baker, 1998a, b; Zhan and Baker, 2006; Song and Baker, 2007; Li et al., 2014). In addition, area LM is the primary target of V1 projections (Wang et al., 2012) and prefers lower spatial frequencies than V1 (Marshel et al., 2011).

The mirrored progression of retinotopy along the azimuth in the two areas provided the advantage to verify that my recording sites were indeed in areas V1 and LM. For recordings, I used a 4-shank silicon probe (See "Material and methods" Fig. 1*b,c*) spanning a large range of azimuths in either area and mapped RFs by presenting a sparse-noise stimulus (**Figure 4**). In order to obtain RF maps individually for each neuron, two-dimensional Gaussians were fitted to the maps of average firing rates (**Figure 4***a,d*, top), separately for ON and OFF stimuli (**Figure 4***a,d*, middle). Finally, I

considered only RFs with well-fit Gaussian profiles and extracted the average azimuth and elevation per shank for those RFs (**Figure 4***b,e,* gray). Considering the fact that RF locations in mouse cortex are considerably scattered (Smith and Hausser, 2010; Bonin et al., 2011), I also analyzed the MUAe (Super and Roelfsema, 2005) for which I determined the peak RF coordinates for each electrode shank (**Figure 4***a,d*, bottom, *b,e*, black). Similar to previous results on the retinotopy of mouse visual areas (Schuett et al., 2002; Wang and Burkhalter, 2007), I found that in V1 area, going from the most medial to the most lateral electrode shank, the azimuth of RF centers shifted from more peripheral to more central (**Figure 4***c*); whereas, conversely, in LM recordings, the azimuth of RF centers moved from more central to more peripheral (**Figure 4***f*).

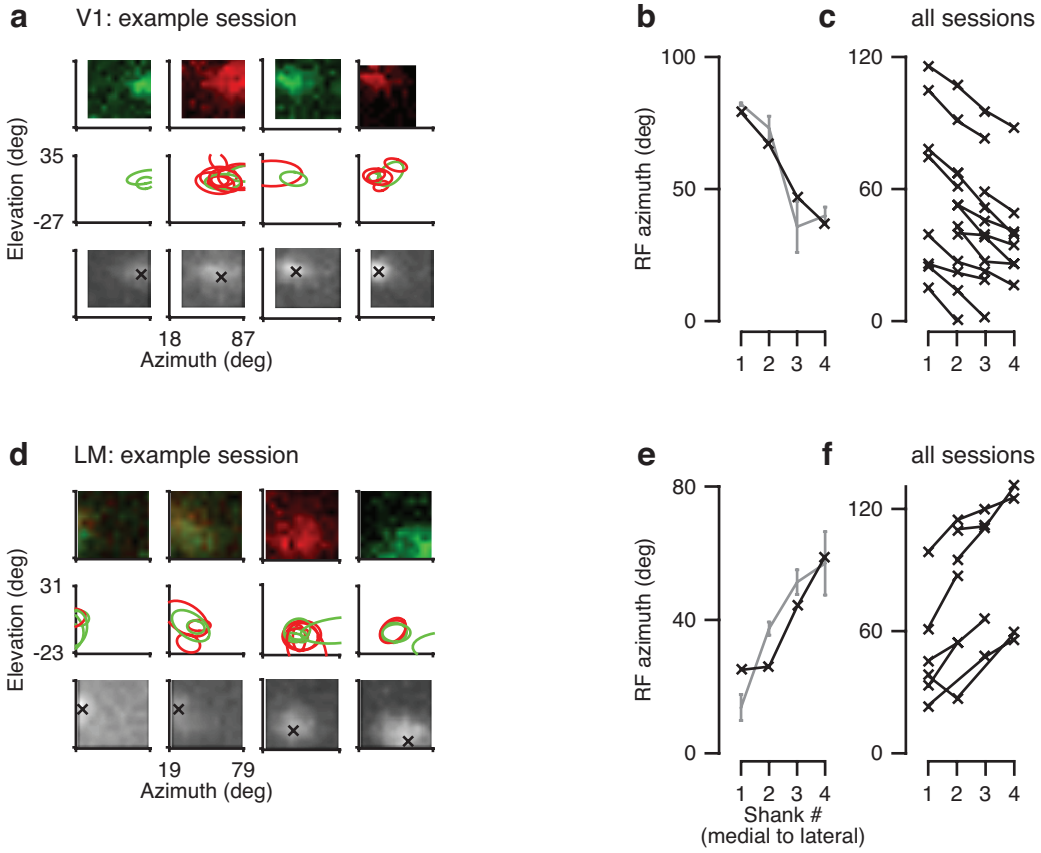

Figure 4. Identification of visual areas V1 and LM by mirrored retinotopic progression of azimuth. ***a***, Top, Example single-unit RF maps in area V1 for each electrode shank in one example session. Red represents ON field. Green represents OFF field. Units 291-2-x.17, 46, 62, 76. Middle, Contours of all well-fitted RFs in this example session. Bottom, RF maps based on multiunit activity for this example session. ***b***, RF azimuth in the example session based on average single-unit RF centers (gray) and multiunit activity (black). ***c***, Summary of RF azimuth across all V1 recordings. *N* = 14 sessions. ***d–f***, Same as ***a–c***, for area LM. Units 241-4-x.47, 67, 70, 84. *f*, *N* = 8 sessions.

Responses to contrast-modulated gratings are weaker and less selective

After verifying the identity of the targeted area, I presented visual stimuli on the center of mapped multiunit RFs and measured the orientation tuning curves of neurons in response to *LGs* and *CGs*. Then, I compared the neural responses to *LGs* and *CGs* across areas V1 and LM. Consistent with previous studies in higher-order mammals (Albright, 1992; Zhou and Baker, 1994; Mareschal and Baker, 1998a; Zhan and Baker, 2006; Li et al., 2014), I found that a considerable percentage of neurons did not respond to *CGs*, despite significant responses to *LGs* (**Figure 5**).

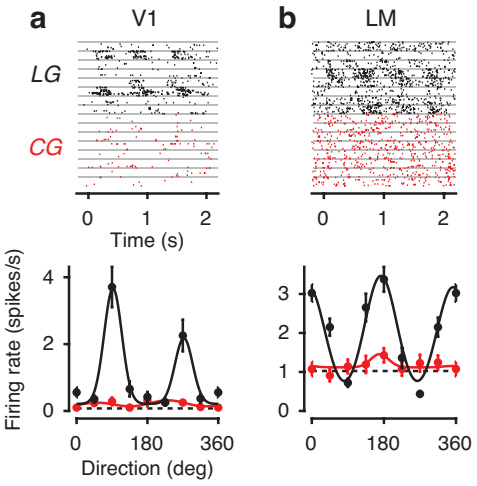

Figure 5. Example neurons unresponsive to *CGs* despite significant responses to *LGs*. ***a***, Activity evoked by *LGs* (black) and *CGs* with low-frequency noise (red) of an example neuron from area V1. Top, Raster plots. Each gray horizontal line separates trials with different stimulus orientations. Bottom, Tuning curves of the same example neuron (Unit 280-2-4.61). Dashed horizontal line indicates response to gray screen; solid lines indicate fit of a sum-of-Gaussians model. ***b***, Same, for an LM example neuron (Unit 245-5-10.35).

Responses to low-frequency noise contrast-modulated gratings

I interleaved *LGs* and *CGs* with low-frequency noise carrier in 8 different orientations and compared the responses orientation tuning curves in response to *LGs* and *CGs* with low-frequency noise, across areas V1 and LM. Among all recorded neurons, only 72% of luminance-responsive neurons also responded to the *CGs* with low-frequency noise (**Figure 6**). The contribution of neurons, which were responsive not only to *LGs* but also to *CGs* with low-frequency noise as well, was higher in V1 (77%, 178 of 230 recorded neurons) than in LM (61%, 69 of 114 recorded neurons, $p < 0.001$, two-way interaction, log-linear analysis; **Figure 6**). Further analysis was performed only on those neurons with a significant response to both types of stimuli.

Among those neurons with significant responses to both *LGs* and *CGs*, example neurons in both V1 (**Figure 7***a*) and area LM (**Figure 7***b*) showed lower peak firing rates in response to *CGs* with low-frequency noise than to *LGs*. In the population of neurons, a similar pattern of reduced peak firing rates to *CGs* was observed. Peak responses across both V1 and area LM decreased by 27.8 ± 3.2%, from 11.2 spikes/s in response to *LGs* to 8.1 spikes/s in response to *CGs* (ANOVA, main effect, $p < 10^{-16}$; **Figure 7***c*,*d*). This reduction was less pronounced in area V1 (25.9 ± 3.1%) than in area LM (31.8 ± 7.3%; interaction, $p < 0.065$). I also found that the responses to the orthogonal orientation for *CGs* versus *LGs* were similar in area V1 (mean change 1.6 ± 0.5%), while LM neurons, more consistently, showed a reduction in their *CGs* responses (mean change −18.6 ± 6.3%; interaction $p = 0.0002$; **Figure 7***e*,*f*).

This pattern of changes in the responsiveness was reflected in the orientation selectivity, both in the example cells (**Figure 7***a*,*b*) and in the population (**Figure 7***g*,*h*): neurons in both areas showed poorer orientation selectivity in response to *CGs* with low-frequency noise carriers compared to *LGs*. To measure orientation selectivity, I computed d', which does not only take into account the difference between responses to preferred and orthogonal orientations but also the variability of responses (Berens, 2009). Comparing orientation selectivity across V1 and area LM revealed, overall, a lower d' for LM than for V1 (main effect, $p = 0.003$). More importantly, d' was lower for

CGs than *LGs* (main effect, $p < 10^{-16}$), and this reduction was more prominent for V1 (60.8 ± 4.5% from 1.39 for *LGs* to 0.54 for *CGs*) than LM (52.0 ± 6.9% from 0.99 for *LGs* to 0.47 for *CGs*; interaction, p = 0.003). Therefore, responses to *CGs* with low-frequency noise carriers compared with *LGs* in mouse visual cortex are weaker and orientation selectivity was poorer.

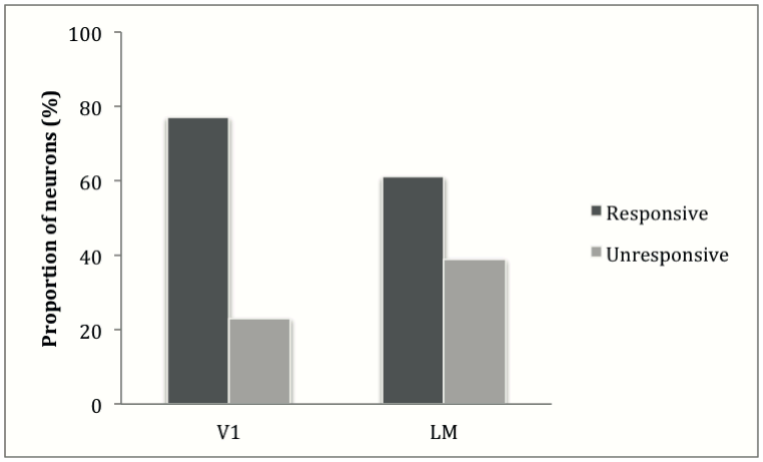

Figure 6. Distribution of responsive and unresponsive neurons to *CGs* with low-frequency noise carrier in V1 (*N* = 230) and area LM (*N* = 114).

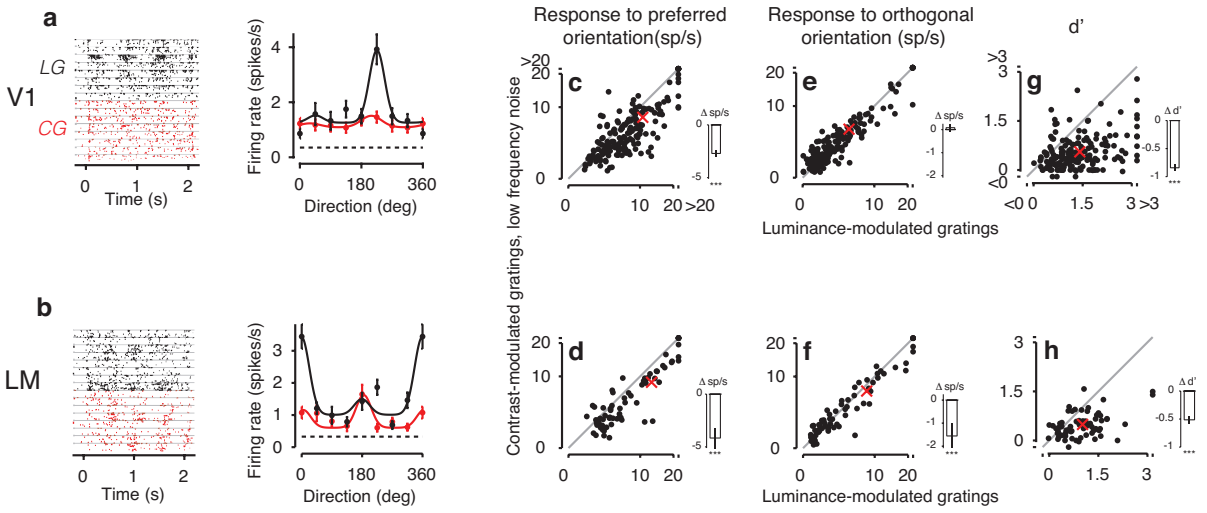

Figure 7. Responses to *CGs* with low-frequency noise carriers in mouse visual cortex. ***a***, Responses to *LGs* (black) and *CGs* (red) of an example neuron from area V1. Top, Raster plots. Bottom, Tuning curves of the same example neuron (Unit 221-1-7.61). ***b***, Same, for an LM example neuron (Unit 245-4-6.35). ***c***, ***d***, Response to the preferred orientation for *CGs* versus *LGs* in the population of responsive neurons recorded from V1, *N* = 178 (***c***) and LM, *N* = 69 (***d***). Insets, Mean pairwise differences and their SEM (Franz and Loftus, 2012). Stars represent significance of *post hoc* comparisons. ***e***, ***f***, Same as ***c***, ***d***, for response to orthogonal orientation. ***g***, ***h***, Same as ***c***, ***d***, for d' . Red crosses represent means. Conventions as in **Figure 5**.

Responses to RMS matched contrast luminance-modulated gratings

To test whether the weaker responses and broader orientation tuning for *CG* than *LG* responses could be explained by the lower RMS contrast of *CG* gratings, I performed control experiments (**Figure 9**). In these experiments, the RMS contrast of *LGs* was matched with that of *CGs*, and responses to this type of *LGs* were measured. In V1 area only 71% of responsive neurons to *LGs* with matched RMS contrast also responded to

the *CGs* with low-frequency noise, this fraction was 76% in area LM (**Figure 8**). Comparing responses to preferred orientation between *CGs* and *LGs* matched in RMS contrast revealed again weaker responses to *CGs* than *LGs* in both areas (7.3 spikes/s vs. 8.8 spikes/s, main effect, $p < 10^{-5}$; **Figure 9**), however, this reduction in responsiveness was less pronounced compared to conditions with full contrast *LGs* (27.8 ± 3.2%; compare **Figure 7***c,d* and **Figure 9***c,d*; interaction, $p = 0.009$). I also found that in area V1, *CGs* evoked stronger responses to orthogonal orientations than *LGs* (4.41 sp/s vs 3.65 sp/s, 20.9 ± 4.2%), however this was not the case for area LM, i.e. the responses to orthogonal orientations did not differ significantly between *LGs* and *CGs* (8.5 sp/s vs 8.7 sp/s, 2.1 ± 4.7%; interaction, $p < 0.01$). Overall d' was again lower for area LM (0.62± 0.05) than V1 (0.86±0.06; main effect, $p = 0.026$), even with matched RMS contrast. Similar to our results with full-contrast *LGs*, d' dropped considerably between *LGs* matched in RMS contrast and *CGs* (66.2 ± 5.5%, from 1.2 for *LGs* to 0.4 for *CGs*, main effect, $p < 10^{-16}$), while d' was not significantly different between responses to full-contrast and reduced-contrast *LGs* ($d'_{full} = 1.3$, $d'_{matched} = 1.2$; compare **Figure 7***g,h* and **Figure 9***g,h*; two-sample t test, $p = 0.4$), which is probably reminiscent of the well-known phenomenon of contrast invariance of orientation tuning (Movshon et al., 1978; Albrecht and Hamilton, 1982; Sclar and Freeman, 1982). Interestingly, reductions in orientation selectivity (d') between *CGs* and *LGs* with matched RMS contrast were more prominent in area V1 (68.3 ± 6.0%, from 1.3 to 0.41) than in area LM (56.3 ± 11.5%, from 0.86 to 0.38; interaction, $p = 0.008$).

Together, the reduced RMS contrast of *CGs* might explain the weaker responses to *CGs* but cannot account for the poorer orientation selectivity for *CGs*. Instead, the broader distribution of orientation energy in *CGs* compared with *LGs* might partially be responsible for poorer orientation selectivity for *CGs* (**Figure 1***,b*).

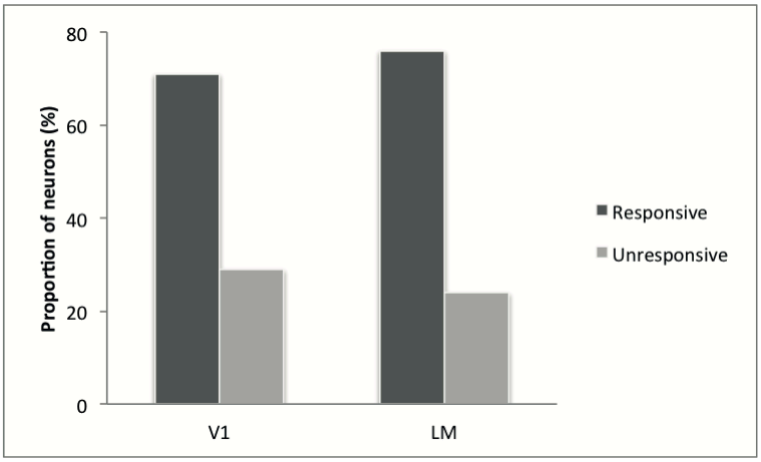

Figure 8. Distribution of responsive and unresponsive neurons to *CGs* with low-frequency noise carrier in RMS-matched contrast *LGs* experiments, in area V1 ($N = 105$) and LM ($N = 59$).

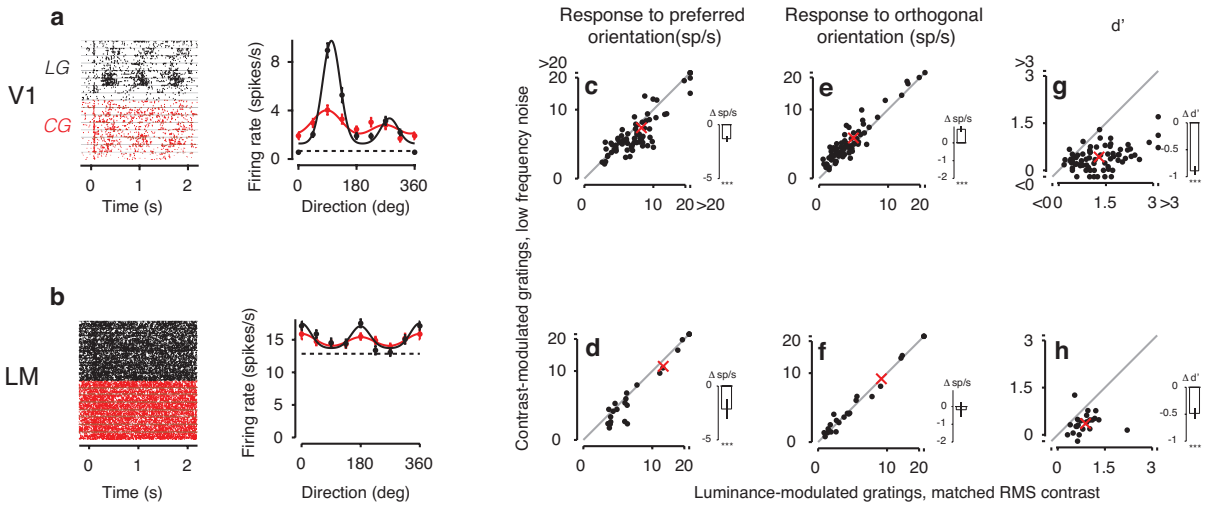

Figure 9. Comparison of responses to *LGs* matched in RMS contrast and *CGs*. ***a***, Responses to *LGs* with matched RMS contrast (black) and *CGs* with low-frequency noise (red) of an example neuron from area V1. Top, Raster plot. Bottom, Tuning curves of the same example neuron (Unit 221-1-6.24). ***b***, Same, for an LM example neuron (Unit 245-5-7.17). ***c***, ***d***, Responses to preferred orientations for *CGs* versus *LGs* with matched RMS contrast in the population of (***c***) V1 neurons, *N* = 73 and (***d***) LM neurons, *N* = 23. ***e***, ***f***, Same as ***c***, ***d***, for responses to orthogonal orientations. ***g***, ***h***, Same as ***c***, ***d***, for d' . Conventions as in **Figure 7**.

Responses to high-frequency noise contrast-modulated gratings

Given that first-order, luminance-sensitive mechanisms in V1 and LM might contribute to the responses to *CGs* with low- frequency noise, I performed additional experiments to test the level of this contribution. Indeed, my findings of weaker responses to preferred orientations of *CGs*, of stronger responses to orthogonal orientations and of poorer orientation tuning compared with *LGs* are consistent with a potential activation of luminance-sensitive mechanisms. To decrease the local orientation-biased luminance fluctuations of the *CGs* in the preferred range of spatial frequency for V1 and LM neurons, I imposed a low-frequency cutoff on the noise carrier such that the noise carrier's spatial frequency distribution was concentrated beyond the passband of many V1 and LM neurons (mean high-cutoffs of 0.07 and 0.055 cycles/degree) (Marshel et al., 2011) and also the differential energy at the orientation domains of the *LGs* across spatial frequencies was little (**Figure 1***a,c*). Then I compared the orientation tuning curves for *LGs* and *CGs* with high-frequency noise carrier across areas V1 and LM.

Among all recorded neurons with significant responses to *LGs*, less than half of them also responded to *CGs* with high-frequency noise carrier (37%, 51 of 139 recorded neurons; **Figure 10**). In comparison, *CGs* with low-frequency noise carrier evoked responses in a larger population (72%, $p < 10^{-11}$, log-linear analysis, interaction). Interestingly, this reduction of responsiveness between two types of *CGs* stimuli was more prominent in area V1 (77% vs. 36%, 29 of 81 recorded neurons) than in area LM (61% vs. 38%, 22 of 58 recorded neurons; $p = 0.040$, log-linear analysis, interaction; compare **Figure 6** and **Figure 10**).

Again, a similar pattern of results was observed in the responses to *LGs* and high-frequency noise carrier *CGs* (**Figure 11**). In both example neurons and in the population of recorded neurons (**Figure 11***a,b*) responses to *CGs* with high-frequency noise carrier were lower than to *LGs*. This reduction was mediated by reduced responses to both the preferred orientation (decrease of 49.2 ± 9.8%, from 13 sp/s to 6.6 sp/s; ANOVA, main effect, $p < 10^{-5}$; **Figure 11***c,d*) and orthogonal orientation (decrease of 29.0 10.4%, from 7.6 sp/s to 5.4 sp/s; ANOVA, main effect, $p = 0.008$; **Figure 11***e,f*). Similarly, d' dropped

considerably by 71.6 ± 6.7% for *CGs* with high-frequency noise compared with *LGs* (from 1.34 to 0.38; ANOVA, main effect, $p < 10^{-13}$; **Figure 11***g*,*h*).

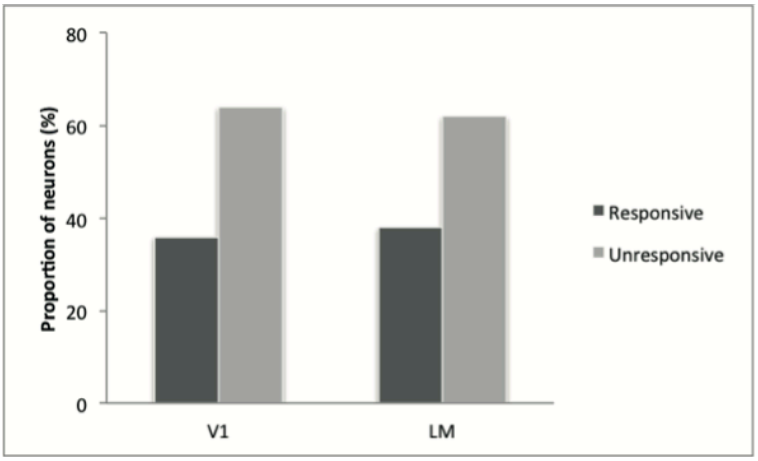

Figure 10. Distribution of responsive and unresponsive neurons to *CGs* with high-frequency noise carrier in area V1 (*N* = 81) and LM (*N* = 58).

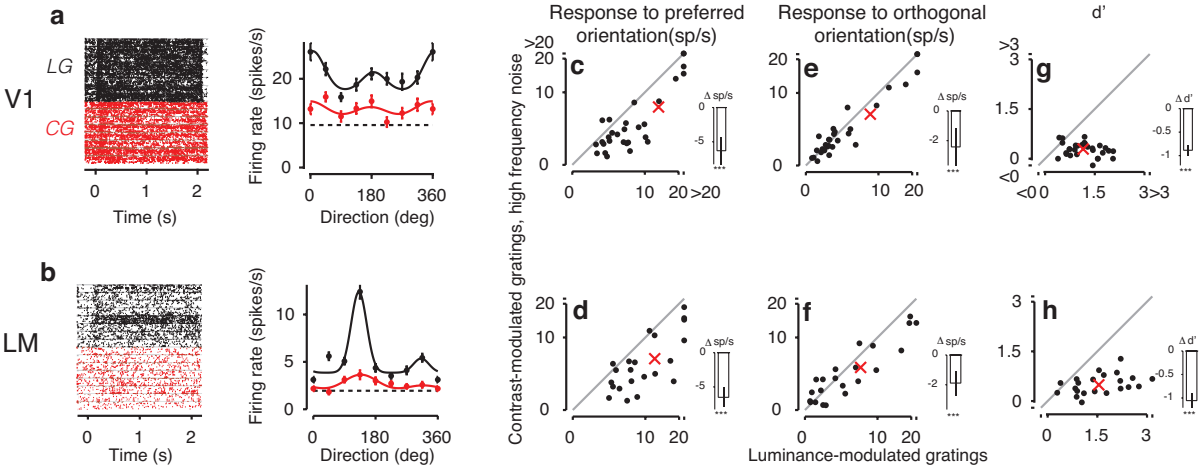

Figure 11. Responses to *CGs* with high-frequency noise carrier. ***a***, Responses to *LGs* (black) and *CGs* with high-frequency noise (red) of a V1 example neuron. Top, Raster plots. Bottom, Tuning curves of the same example neurons (Unit 326-1-2.48). ***b***, Same for an LM example neuron (Unit 299-3-13.42). ***c***, ***d***, Responses to preferred orientations for *CGs* with high- frequency noise versus *LGs* in the population of V1 neurons, *N* = 29 (***c***) and LM neurons, *N* = 22, (***d***). ***e***, ***f***, Same as ***c***, ***d***, for responses to orthogonal orientations. ***g***, ***h***, Same as ***c***, ***d***, for d' . For other conventions, see **Figure 7**.

Preferred orientations for luminance-modulated and contrast-modulated gratings are broadly similar

Finally, to test the potential contribution of *CG* representation in the cue-invariant perception of stimulus orientation, I compared the neurons' preferred orientation, separately for each grating type (**Figure 12**). Given the fact that stronger orientation selectivity will entail a more accurate estimate of preferred orientation, I considered only those neurons with d' > 1 for *LGs* (**Figure 12,** black circles). First, I examined the degree of uniformity in the distribution of differences in preferred orientations for *LGs* and *CGs*. I observed that the distribution of differences in preferred orientation between *LGs* and *CGs* with low-frequency noise (**Figure 12** *a,b*) was not uniform in both area V1 (Rayleigh test, $p < 10^{-10}$) and LM (Rayleigh test, $p = 0.03$). Indeed, in both areas V1 (0.43, $p < 10^{-4}$) and LM (0.4, $p = 0.02$), preferred orientation for *CGs* with low-frequency

noise and *LGs* were correlated. However, the residual activation of luminance-sensitive mechanisms by the *CGs* with low-frequency noise also could give rise to similar results. Interestingly, for *CGs* with high-frequency noise (**Figure 12***c,d*), the differences in preferred orientation were distributed non-uniformly only for area LM (Rayleigh test, $p = 0.005$) and correlations between preferred orientations were observed only for area LM (0.58, $p = 0.02$). This finding is remarkable, as LM neurons, with their preferences for lower spatial frequencies (Marshel et al., 2011), are expected to be less sensitive to any residual orientation signal potentially present at higher spatial frequencies. As the last step, I performed control experiments to assess how much of the observed scatter of preferred orientations arises from estimation errors due to limited data. In these control experiments, only *LGs* were presented and all other aspects of experiments and analyses were left identical (**Figure 12***e,f*). I observed that only little variability arose from limited data, at least for the strongly tuned neurons. Together, my finding of broadly similar preferred orientation between grating types provides some evidence for a coarse cue-invariant, which might partially be the neural correlates for perceptual generalization of orientation discrimination.

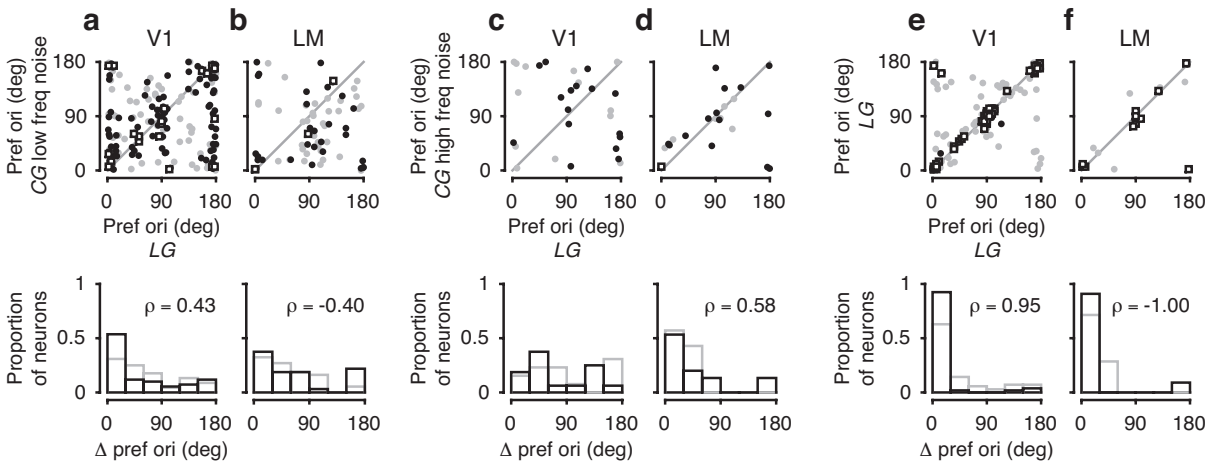

Figure 12. Comparison of preferred orientation for contrast-modulated versus *LGs*. ***a***, Top, Preferred orientations of V1 neurons in response to *CGs* with low-frequency noise carrier versus *LGs*. Bottom, Distribution of differences in preferred orientations. Black represents neurons with d' >1 for *LGs* ($N = 110$). Gray represents neurons with d' < 1 ($N = 68$). Square markers represent neurons with d' > 1 for both grating types. ***b***, Same as ***a***, for LM neurons ($N = 32$ with d'> 1 and $N = 37$ with d' < 1). ***c***, Same as ***a***, but for *CGs* with high-frequency noise carrier versus *LGs* (V1, $N = 16$ with d' > 1 and $N = 13$ for d' < 1). ***d***, Same as ***c***, for LM neurons ($N = 15$ with d' > 1 and $N = 7$ for d' < 1). ***e***, Same as ***a***, but repeating the *LG* condition (V1, $N = 53$ with d' > 1 and $N = 70$ with d' < 1). ***f***, Same as ***e***, for LM neurons ($N = 11$ with d' > 1 and $N = 7$ with d' < 1).

Responses to contrast-modulated gratings during anesthesia

I also performed extracellular recordings under anesthesia, in which I measured the orientation tuning in response to *LGs* and *CGs* with low-frequency noise carrier across both areas V1 and LM. The pattern of results was similar to those during wakefulness, such that both V1 and LM neurons were less responsive and selective to *CGs* than *LGs*. Indeed, about half of all recorded neurons in both V1 and area LM did not respond to *CGs* despite their significant responses to *LGs* (**Figure 13**). The fraction of responsive neurons to both *LGs* and *CGs* (49%) was lower compared to during wakefulness (72% $p < 0.001$, interaction, log-linear analysis). The reduction of responsiveness with brain state was similar for LM (awake: 61% vs. anesthetized: 42%) and V1 (awake: 77% vs.

anesthetized: 64%; three-way interaction, p = 0.85). The fraction of responsive neurons to second-order stimuli during anesthesia was higher in V1 (64%) than in LM (42%, p < 0.001, interaction, log-linear analysis; **Figure 14**).
Among those neurons with significant responses to both *LGs* and *CGs*, example neurons in both areas V1 (**Figure 15***a,c*) and area LM (**Figure 15***b,d*) had lower peak firing rates for *CGs* compared to *LGs*. This reduction of firing rates to *CGs* was also evident in the population of recorded neurons, where I used an ANOVA to test statistical significance. Responses across recorded areas dropped by 36.1% ± 5.2, from 9.8 spikes/s in response to *LGs* to 6.3 spikes/s in response to *CGs* (ANOVA, main effect, $p < 10^{-8}$, **Figure 15***e-h*). I also noted that the responses to the orthogonal orientation for *CGs* versus *LGs* decreased in both areas (area V1, mean change 25.3% ± 8.3; area LM, mean change 21.1% ± 5.7; main effect, $p < 10^{-4}$).

This decrease in responsiveness was accompanied by a concomitant drop in selectivity for stimulus orientation for *CGs*, both in the example cells (**Figure 15***a-d*) and in the population during anesthesia (**Figure 15***i-l*). d' was lower during anesthesia than wakefulness (main effect, p < 0.01). More importantly, d' during anesthesia was higher for LM than V1 (main effect, p = 0.03) and lower for *CGs* than *LGs* (main effect, $p < 10^{-08}$), and this difference tended to be stronger for LM (69.7% ± 13.9 from 1.22 for *LGs* to 0.36 for *CGs*) than V1 (57.3% ± 12.9) from 0.76 for *LGs* to 0.32 for *CGs*, interaction, p = 0.05). Thus, responses to *CGs* compared to *LGs* in mouse visual cortex during anesthesia are lower and less selective for orientation.

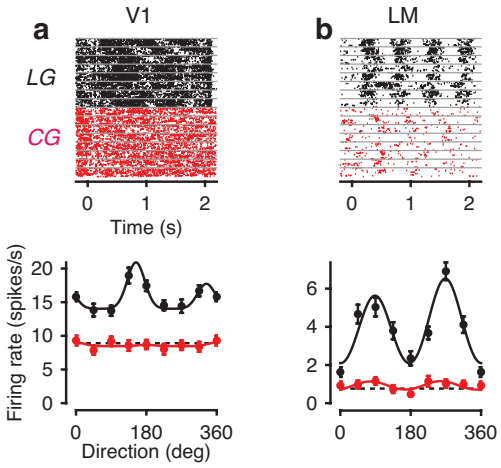

Figure 13. Example neurons unresponsive to *CGs* despite significant responses to *LGs* during anesthesia. ***a***, Activity evoked by *LGs* (black) and *CGs* with low-frequency noise (red) of an example neuron from area V1. Top, Raster plots. Each gray horizontal line separates trials with different stimulus orientations. Bottom, Tuning curves of the same example neuron (Unit 232-5-8.23). Dashed horizontal line indicates response to gray screen; solid lines indicate fit of a sum-of-Gaussians model. ***b***, Same, for an LM example neuron (Unit 242-2-12.35).

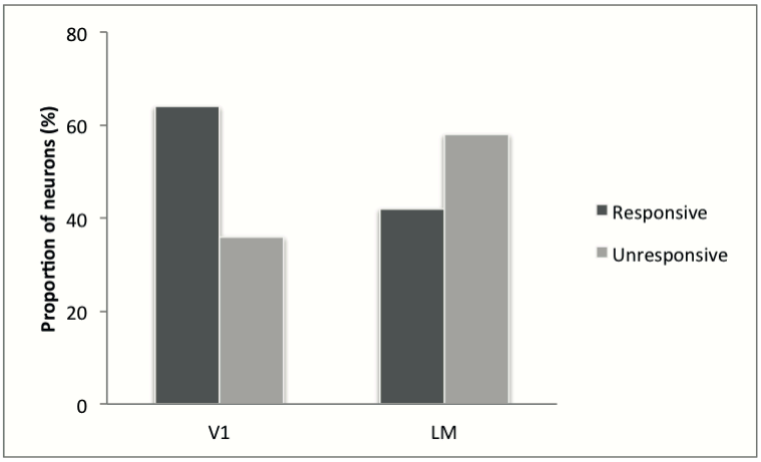

Figure 14. Distribution of responsive and unresponsive neurons to *CGs* with low-frequency noise carrier in area V1 (*N* = 55) and LM (*N* = 100) during anesthesia.

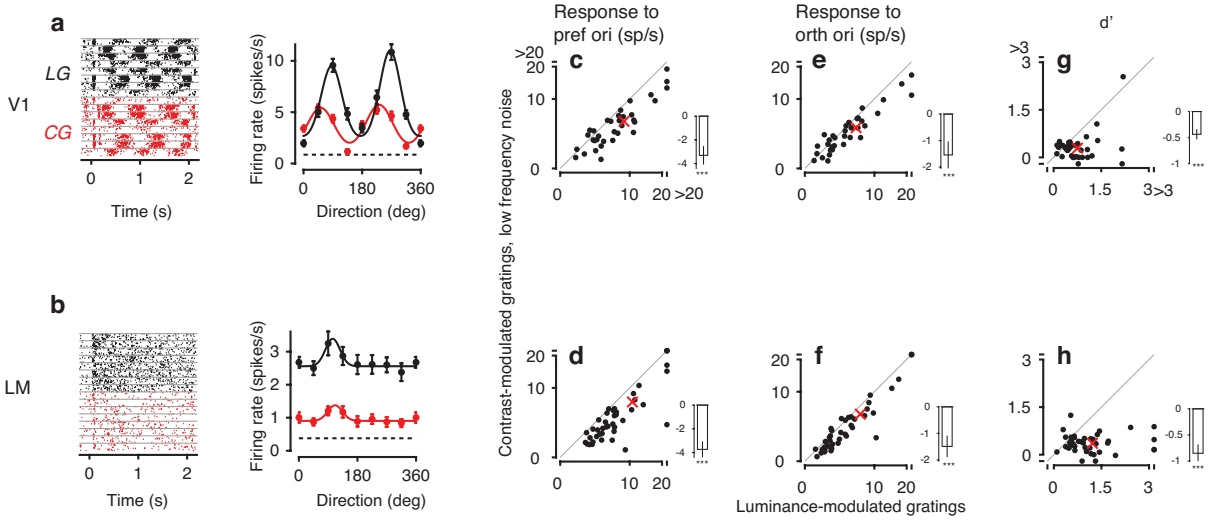

Figure 15. Responses to *CGs* with low-frequency noise carriers in mouse visual cortex during anesthesia. ***a***, Responses to *LGs* (black) and *CGs* (red) of an example neuron from area V1. Top, Raster plots. Bottom, Tuning curves of the same example neuron (Unit 232-5-4.6). ***b***, Same, for an LM example neuron (Unit 144-2-20.39). ***c***, ***d***, Response to the preferred orientation for *CGs* versus *LGs* in the population of responsive neurons recorded from V1, *N* = 178 (***c***) and LM, *N* = 69 (***d***). ***e***, ***f***, Same as ***c***, ***d***, for response to orthogonal orientation. ***g***, ***h***, Same as ***c***, ***d***, for d'. Conventions as in **Figure 7**.

Discussion

In this thesis, I investigated whether mice can use second-order stimuli in a cue-invariant way to guide visual perception during an orientation discrimination task, and screened for potential neural correlates in mouse visual cortex. I found that mice could readily generalize orientation discrimination learning from the familiar cue condition of luminance-modulated gratings (*LGs*) to a novel cue condition of contrast-modulated gratings (*CGs*), albeit with a substantial decrease in performance. My electrophysiological data supported these behavioral results: in both areas V1 and LM, the population of responsive neurons to *CGs* was less than that of *LGs*. Furthermore, responses to *CGs* were generally weaker and less orientation selective than to *LGs*. Despite these differences, preferred orientations were broadly similar in response to both *LGs* and *CGs*, pointing to a potential underlying mechanism of the basic cue-invariant generalization in mouse orientation discrimination performance. My observation of cue-invariance might provide the basis for object recognition and categorization invariant to changes in object appearance, as recently demonstrated in rats (Zoccolan et al., 2009; Tafazoli et al., 2012; Vermaercke and Op de Beeck, 2012; Alemi-Neissi et al., 2013; Vinken et al., 2014; De Keyser et al., 2015).

Choice of paradigm

From previous behavioral studies on the limits of rodent vision, it has become clear that the particularity of the paradigm can strongly influence the measured visual abilities. For example, Busse and her colleagues in 2011 (Busse et al., 2011) used a nose-poke two-alternative forced task (2AFC) to measure mice contrast sensitivity at preferred spatial frequency and reported 20% contrast threshold, whereas a much lower contrast threshold (2%) was estimated when a yes-no paradigm was used, instead (Histed et al., 2012). The discrepancy present between these two studies might partly be explained by the difference in both the level and the stability of animals' motivation between 2AFC and yes-no paradigms. In the yes-no paradigm used in Histed's study not only mice' performance was close to optimal but more importantly it was stable across different sessions of training, as well. Indeed, measuring psychometric functions in an operant, lever-pressing paradigm provided the opportunity to detect any changes in animals' motivation, arousal or attention and it revealed negligible, near to zero, lapse rates. Moreover, their estimates of threshold were repeatable across sessions and mice, indicating stability in performance and little deviation (if at all) from optimal behavior. In contrast, in the 2AFC paradigm used by Busse et al., mice' performance was influenced by non-sensory factors such as past history of failures and rewards and estimates of reward values and thus by fluctuations in animals' motivation. To sum up, estimates of mouse contrast sensitivity in a nose-poke 2AFC task do not exclusively reflect perceptual limits, as it can also be limited by non-sensory factors (Busse et al., 2011), whereas rigorous psychophysical measurements using a lever-press paradigm under head fixation can reveal perceptual thresholds that are less influenced (Histed et al., 2012).

Why did I choose classical conditioning?

In order to test whether mouse vision is capable of perceiving *CGs*, despite its low acuity, I chose a classical conditioning paradigm. Following Gallistel et al. (2004), and by

performing a quantitative analysis on conditioned responses (*LIs*) I was able to compare mouse behavior before vs. during *CGs* presentations. The positive slope of cumulative records of conditioned responses (*LIs*) indicated that mice have stronger conditioned responses during *CGs* presentation than before, which simply confirms *CGs* perception. Furthermore, classical conditioning allowed me to test separately *CGs* perception and *CGs* orientation discrimination abilities in mice. The difference between *LIs* to rewarded and unrewarded *CGs* orientations, demonstrated orientation discrimination capability of mice for *CGs*, albeit with a substantial drop in performance. Therefore, employing classical conditioning provided, for my study, the advantage of a distinct behavioral read-out for the visibility of the stimulus and discriminability of its orientation.

Can classical conditioning paradigm reveal the limits of visual performance?

Despite offering the advantage outlined above, classical conditioning might not be able to measure near-threshold performance in my task, due to potential fluctuations in motivational states of animals. As explained earlier, any fluctuation of animal motivation could strongly influence on experimental results and be misleading to estimate visual limits (Busse et al., 2011; Histed et al., 2012). In the other paradigms such as touch screen panels (Bussey et al., 2001), and operant lever-pressing (Histed et al., 2012) which require mice to initiate the trial or participate actively in the experiment to obtain reward, the animals' attention and motivation might be more stable, the animals' performances might be less contaminated and might reflect accurately the perception limits. In contrast, classical conditioning, despite offering powerful insights into several aspects of visual perception, can involve more reflexive behavior and trial-to-trial fluctuations in motivation cannot be excluded. Therefore, I speculate that using other paradigms, such as operant lever-pressing (Histed et al., 2012) or touch screen panels (Bussey et al., 2001), might result in a better performance for orientation discrimination of *CGs* compared to what I observed during classical conditioning in this project. Indeed, a reasonable behavioral generalization of first- to second-order stimuli was observed recently in rats trained in a touch-screen paradigm (De Keyser et al., 2015). In addition, one type of invariant visual object recognition has been reported during an operant paradigm, where rats had to recognize the objects despite a range of changes in size and positions. In this type of paradigm, rats were trained to initiate each trial by inserting their head into a whole in front of training box (Alemi-Neissi et al., 2013).

It is important to note that despite my finding that mice are able to generalize the learned orientation discrimination task from *LGs* to *CGs*, this generalization was rather limited. First, not only did discrimination performance substantially drop from *LGs* to *CGs*, but extensive training also did not lead to a qualitatively better performance during *CGs*. Second, I tested one mouse who was never able to reliably discriminate *CGs* even after prolonged sessions of training. Third, I realized that the wave shape of *LGs* determines successful transfer of learning to *CGs* later. Indeed, mice were able to generalize from *LGs* to *CGs* only after being initially trained with sine-wave *LGs*, but never after being initially trained with square-wave *LGs*. All 3 mice trained initially with square-wave *LGs*, could no longer discriminate orientation when the gratings were contrast modulated, despite being able to see the grating, as they showed unspecific

conditioned responses to *CGs*' presence. Indeed, these mice could see *CGs* but failed to discriminate different orientations.

Underlying mechanism of second-order

As I showed in this study, neurons in both area V1 and LM not only respond to *CGs* but also are orientation-selective for *CGs*. Furthermore, comparing the preferred orientation of V1 and LM neurons to *LGs* and *CGs* revealed a coarse correspondence between them. Therefore, my electrophysiological data could potentially underlie the perceptual generalization of orientation discrimination from *LGs* to *CGs*. Previous studies in higher-order mammals guided by rich knowledge of the spatiotemporal properties across visual areas (Movshon et al., 1978; Issa et al., 2000) suggested a two-stage filter model for second-order processing. In this filter-rectify-filter model, the first linear spatial filter detects the fine structures of second-order stimuli and then its output is transferred to a nonlinear rectifier, and finally, the second linear spatial filter sums up the rectified responses. However, the neural substrates underlying these three stages remain controversial, particularly those pertaining to the first filter. An electrophysiological study in area V2 of monkeys has proposed that small receptive fields in V1, tuned to spatial frequency and orientation, act as a potential neural substrate for the first linear filter (Li et al., 2014), while another study in cats (Rosenberg et al., 2010; Rosenberg and Issa, 2011) reported nonlinear responses and tuning to carrier spatial frequency and orientation of *CGs* in LGN Y-cells, suggesting that subcortical structures, i.e. LGN, could also serve as first stage filter. Regarding the neural substrate of the second filter, it has been suggested that V2 neurons which have bigger receptive fields than V1 neurons and consist of V1 receptive fields sum up the rectified responses coming from primary visual area's RF and provide the orientation selectivity (Li et al., 2014). However, it is uncertain yet whether primate or carnivore brain possesses such second-order processing stages or whether mechanisms other than filter-rectify-filter, such as surround-suppression, explain the second-order responses (Tanaka and Ohzawa, 2009; El-Shamayleh and Movshon, 2011; Hallum and Movshon, 2014; Li et al., 2014). Tanaka and Ohzawa (2009) suggested that neural responses to a second-order stimuli in area 17 of cats arise from surround suppression, however, measuring the suppression index of V2 neurons showed little or no surround suppression for half of second-order responsive neurons. Furthermore, employing high ratio of carrier spatial frequency to envelope frequency indicated that the second-order responses could potentially be explained by filter-rectify-filter mechanism instead (Li et al., 2014). My findings of cue-invariant responses to *CGs* in mice cannot resolve this debate, as the stimulus I used cannot determine accurately the source of those responses. The observed cue-invariant responses to *CGs* used in this study could potentially emerge either from residual activation of luminance-sensitive mechanisms or could be mediated by suppressive mechanisms from the surround (Tanaka and Ohzawa, 2009; Hallum and Movshon, 2014). Nevertheless, the pattern of LM responses to high-frequency noise carrier *CGs* is reminiscent of the filter-rectify-filter framework (see below).

Potential role of LM in perception of texture boundaries

The electrophysiological data that I acquired in this project points towards a potentially interesting role of area LM in the perception of texture boundaries. As I showed in this study, LM neurons in mice not only respond to *CGs* with high-frequency noise carriers,

but also maintain some orientation selectivity to these *CGs*. More importantly, unlike in V1, neurons in area LM showed a broadly similar preferred orientation for *LGs* and *CGs* with high-frequency noise carriers. This finding is remarkable because first, it is not probable that the high spatial frequency distribution of the noise carrier evokes the luminance-sensitive mechanism and second, area LM should be less sensitive to any residual orientation signal potentially present at higher spatial frequencies (Marshel et al., 2011). These characteristics of LM neurons offer the potential involvement of area LM in the perception of texture boundaries. This potential role of area LM is particularly intriguing, as the properties of area LM fit well with the filter-rectify-filter model: similar to V2 and area 18 in monkeys and cats, LM has been indicated to be a primary projection target of V1 (Levitt et al., 1994; Wang et al., 2011; 2012), has bigger receptive fields (Levitt et al., 1994; Price et al., 1994; Van den Bergh et al., 2010) and shows lower spatial frequency tuning compare to V1 (Movshon et al., 1978a; Foster et al., 1985; Marshel et al., 2011). However, to test explicitly whether filter-rectify-filter mechanisms exist in the mouse visual cortex, further experiments are required to assess precisely the carrier spatial frequencies. In order to exclude any source of luminance-sensitive mechanism in cue-invariant neuronal responses, a carrier with high spatial frequencies unresolvable by the first-order mechanism needs to be employed. In such experiments, one should determine tuning for carrier spatial frequency and aim to rule out any possible source of nonlinear artifacts, which might come either from the display device or the photoreceptors (Zhou and Baker, 1994; Mareschal and Baker, 1998a; Li et al., 2014). These various artifacts either cannot yield such carrier tuning or if they can, it would be the same in every neuron. Therefore, tuning for spatial frequency, which varies across neurons and is distinct from that of the envelope, could ensure that the observed nonlinearity does not emerge from artifacts. In addition, being able to demonstrate a spatial frequency tuning to the carrier distinct from that predicted by a surround mechanism (Tanaka and Ohzawa, 2009) would rule out activation of luminance-sensitive mechanisms (Li et al., 2014).

Are the other mouse extrastriate areas more strongly responsive to second-order stimuli?

I demonstrated that area LM is responsive and orientation selective to second-order stimuli, however, it is not clear whether any of the other mouse extrastriate areas respond more strongly to second-order stimuli. Currently, it is debated whether area LM belongs to the ventral or dorsal stream, despite being identified as a V2 homologous due to its distinct connections and the shared representation of the vertical meridian (Coogan and Burkhalter, 1993; Wang and Burkhalter, 2007). Studies based on cytoarchitectonic and chemoarchitectonic markers and pathway tracing suggested that area LM belongs to ventral stream as it receives its strongest projections from V1 and forwards inputs to limbic areas (e.g. the lateral entorhinal cortex and the amygdala) and also to the superficial layers of the superior colliculus (Wang et al., 2011; Wang and Burkhalter, 2013). Despite being a powerful approach for exploring the interconnectivity and potential function of visual processing streams (Wang and Burkhalter, 2007; Wang et al., 2012), pathway-tracing methods hold some limitations. In fact, the strength of projections to a certain area may not represent precisely the function of neurons in that area. This is because it is not just the number, but also the strength and functional contents of synapses which determine the physiological role of a given structure (De Pasquale and Sherman, 2011). On the other hand, measuring

fundamental properties of extrastriate areas in mouse visual cortex suggests that detailed structure of visual images are analyzed, not by LM, but rather other areas preferring high spatial frequencies such as PM and LI (Andermann et al., 2011; Marshel et al., 2011). Using two-photons calcium imaging, Marshel et al. (2011), measured the fundamental properties of mouse visual areas and suggested that area PM with its high spatial frequency preferences and high orientation selectivity could resemble the primate ventral stream. They also proposed a similar but less dominant role for LI area. However, their results in area LM were less compelling, as LM showed the highest temporal frequency (1.8 HZ) and a moderate spatial frequency (0.028 cycles/ degree) among seven visual areas, which brought them to conclude that area LM is more dorsal-like than ventral-like area. In addition, another study comparing responses to pattern and component motion across different visual areas showed that area LM responds to pattern motion, reminiscent of the dorsal stream, which is in contrast to V1 and AL areas, which are more component-like (Juavinett and Callaway, 2015). To sum up, the functional division of rodent extrastriate areas is a matter of debate and despite the established similarities of mouse vision and primates, it is difficult to assign distinct tasks to each individual area in mouse visual cortex. A recent study in rats investigated the correlation of neural responses in extrastriate areas and behavioral performances in a shape discrimination task and reported that neural responses in higher visual areas represent more behavioral discriminability, while neural responses in V1 area were more closely related to physical differences between visual stimuli (Vermaercke et al., 2015). It is, therefore, likely that other extrastriate areas, which are located in higher levels of the mouse ventral stream hierarchy, respond more strongly to second-order stimuli, as in nonhuman primates (Poort et al., 2012; An et al., 2014). In agreement with this notion, studies in primates which examined motion perception (An et al., 2012) and figure-ground segregation (Poort et al., 2012) across V1 and higher visual areas observed more prominent and stronger responses in V2 and V4 areas than V1 area.

It is also currently unknown whether responses to second-order gratings are stronger during task performance.

Whether performing a task could enhance the second-order responses is not clear. The ideal experiments would be those in which neural responses to both grating types were measured during the orientation discrimination task in both naïve and trained animals. A recent study showed that learning of visual discrimination with first-order gratings modulates the population responses in area V1 (Poort et al., 2015). Indeed, by imaging the population neurons in layer 2/3 of V1, they found that learning enhances the representation of task-relevant stimuli in the population-level in consecutive training sessions. Tracking individual neurons during consecutive training sessions demonstrated that the observed enhancement of neural representations at the population-level occurred via stabilizing the existing and recruiting new neurons selective for task-relevant stimuli. In fact, learning decreases the variability of a given neuron in its selectivity for a certain stimulus (Peters et al., 2014) and in addition, recruits newly selective neurons, which were not selective before learning (Poort et al., 2015). It is also possible that similar alterations occur during learning of other grating types such as second-order stimuli.

Conclusion

To summarize, in this thesis I have examined the processing of different second-order visual stimuli in the mouse model. I found that mice are capable of generalizing orientation discrimination learning from first-order to second-order gratings and their neurons in both V1 and area LM are orientation-tuned to second-order gratings. These results are remarkable, as they offer new insights for future studies to investigate simple forms of invariance and their circuit-level neural mechanisms in the mouse model, where various genetic engineering methods are available for chronic imaging of all visual cortical areas (Andermann et al., 2011; Marshel et al., 2011), causal manipulation of specific cell types (Fenno et al., 2011), and circuit tracing (Wickersham et al., 2007).

Acknowledgment

Firstly, I would like to express my special thanks to my advisor Prof. Laura Busse for the continuous support of my PhD research and for her patience, encouragement and immense knowledge. She has been always academically and emotionally supportive and helpful in last 5 years. Beside my advisor, I would like to thank my committee members, Prof. Thomas Euler, Prof. Cornelius Schwartz and Prof. Uwe Ilg for serving as my committee members even at hardship. A special thanks goes to Prof. Horst Herbert, Prof. Matthias Bethge and Prof. Andreas Bartels for their supports during my PhD. I would like to thank Dr. Reza Daliri, who provided me the opportunity to join Prof. Laura Busse's lab. Without his support would not be possible to conduct this research. I am also grateful to Dr. Steffen Katzner, lab-mates and friends for their kind supports. Last but by no means least, I thank my great family who has been always supportive in my life and during my PhD as well.

References

Albrecht DG, Hamilton DB (1982) Striate cortex of monkey and cat: contrast response function. J Neurophysiol 48:217-237.

Albright TD (1992) Form-cue invariant motion processing in primate visual cortex. Science 255:1141-1143.

Alemi-Neissi A, Rosselli FB, Zoccolan D (2013) Multifeatural shape processing in rats engaged in invariant visual object recognition. J Neurosci 33:5939-5956.

An X, Gong H, Qian L, Wang X, Pan Y, Zhang X, Yang Y, Wang W (2012) Distinct Functional Organizations for Processing Different Motion Signals in V1, V2, and V4 of Macaque. The Journal of Neuroscience 32:13363--13379.

An X, Gong H, Yin J, Wang X, Pan Y, Zhang X, Lu Y, Yang Y, Toth Z, Schiessl I, McLoughlin N, Wang W (2014) Orientation-cue invariant population responses to contrast-modulated and phase-reversed contour stimuli in macaque V1 and V2. PLoS One 9:e106753.

Andermann ML, Kerlin AM, Roumis DK, Glickfeld LL, Reid RC (2011) Functional Specialization of Mouse Higher Visual Cortical Areas. Neuron 72:1025--1039.

Anzai A, Peng X, Van Essen DC (2007) Neurons in monkey visual area V2 encode combinations of orientations. Nat Neurosci 10:1313-1321.

Baker CL, Jr., Mareschal I (2001) Processing of second-order stimuli in the visual cortex. Prog Brain Res 134:171-191.

Berens P (2009) CircStat: A MATLAB Toolbox for Circular Statistics. 2009 31:21.

Berens P, Keliris GA, Ecker AS, Logothetis NK, Tolias AS (2008) Comparing the feature selectivity of the gamma-band of the local field potential and the underlying spiking activity in primate visual cortex. Front Syst Neurosci 2:2.

Bonin V, Histed MH, Yurgenson S, Reid RC (2011) Local Diversity and Fine-Scale Organization of Receptive Fields in Mouse Visual Cortex. The Journal of Neuroscience 31:18506--18521.

Boulanger LM (2009) Immune proteins in brain development and synaptic plasticity. Neuron 64:93-109.

Busse L, Ayaz A, Dhruv NT, Katzner S, Saleem AB, Scholvinck ML, Zaharia AD, Carandini M (2011) The detection of visual contrast in the behaving mouse. J Neurosci 31:11351-11361.

Bussey TJ, Saksida LM, Rothblat LA (2001) Discrimination of computer-graphic stimuli by mice: a method for the behavioral characterization of transgenic and gene-knockout models. Behav Neurosci 115:957-960.

Coogan TA, Burkhalter A (1993) Hierarchical organization of areas in rat visual cortex. J Neurosci 13:3749-3772.

Crook ZR, Housman D (2011) Huntington's Disease: Can Mice Lead the Way to Treatment? Neuron 69:423-435.

De Keyser R, Bossens C, Kubilius J, Op de Beeck HP (2015) Cue-invariant shape recognition in rats as tested with second-order contours. Journal of Vision 15:14-14.

De Pasquale R, Sherman SM (2011) Synaptic properties of corticocortical connections between the primary and secondary visual cortical areas in the mouse. J Neurosci 31:16494-16506.

De Valois RL, William Yund E, Hepler N (1982) The orientation and direction selectivity of cells in macaque visual cortex. Vision Res 22:531-544.

Desimone R, Albright TD, Gross CG, Bruce C (1984) Stimulus-selective properties of inferior temporal neurons in the macaque. J Neurosci 4:2051-2062.

Dombeck DA, Khabbaz AN, Collman F, Adelman TL, Tank DW (2007) Imaging Large-Scale Neural Activity with Cellular Resolution in Awake, Mobile Mice. Neuron 56:43-57.
El-Shamayleh Y, Movshon JA (2011) Neuronal responses to texture-defined form in macaque visual area V2. J Neurosci 31:8543-8555.
Felleman DJ, Van Essen DC (1991) Distributed hierarchical processing in the primate cerebral cortex. Cereb Cortex 1:1-47.
Fenno L, Yizhar O, Deisseroth K (2011) The development and application of optogenetics. Annu Rev Neurosci 34:389-412.
Foster KH, Gaska JP, Nagler M, Pollen DA (1985) Spatial and temporal frequency selectivity of neurones in visual cortical areas V1 and V2 of the macaque monkey. J Physiol 365:331-363.
Franz VH, Loftus GR (2012) Standard errors and confidence intervals in within-subjects designs: generalizing Loftus and Masson (1994) and avoiding the biases of alternative accounts. Psychon Bull Rev 19:395-404.
Freeman J, Ziemba CM, Heeger DJ, Simoncelli EP, Movshon JA (2013) A functional and perceptual signature of the second visual area in primates. Nat Neurosci 16:974-981.
Gallistel CR, Fairhurst S, Balsam P (2004) The learning curve: implications of a quantitative analysis. Proc Natl Acad Sci U S A 101:13124-13131.
Gallistel CR, Mark TA, King AP, Latham PE (2001) The rat approximates an ideal detector of changes in rates of reward: implications for the law of effect. J Exp Psychol Anim Behav Process 27:354-372.
Gao E, DeAngelis GC, Burkhalter A (2010a) Parallel input channels to mouse primary visual cortex. J Neurosci 30:5912-5926.
Gao E, DeAngelis GC, Burkhalter A (2010b) Parallel Input Channels to Mouse Primary Visual Cortex. J Neurosci 30:5912-5926.
Guo ZV, Hires SA, Li N, O'Connor DH, Komiyama T, Ophir E, Huber D, Bonardi C, Morandell K, Gutnisky D, Peron S, Xu NL, Cox J, Svoboda K (2014) Procedures for behavioral experiments in head-fixed mice. PLoS One 9:e88678.
Hallum LE, Movshon JA (2014) Surround suppression supports second-order feature encoding by macaque V1 and V2 neurons. Vision Res 104:24-35.
Hazan L, Zugaro M, Buzsaki G (2006) Klusters, NeuroScope, NDManager: A free software suite for neurophysiological data processing and visualization. Journal of Neuroscience Methods 155:207-216.
Histed MH, Carvalho LA, Maunsell JH (2012) Psychophysical measurement of contrast sensitivity in the behaving mouse. J Neurophysiol 107:758-765.
Holscher C, Schnee A, Dahmen H, Setia L, Mallot HA (2005) Rats are able to navigate in virtual environments. Journal of Experimental Biology 208:561-569.
Hubel DH, Wiesel TN (1959) Receptive fields of single neurones in the cat's striate cortex. J Physiol 148:574-591.
Hubel DH, Wiesel TN (1962) Receptive fields, binocular interaction and functional architecture in the cat's visual cortex. Journal of Physiology 160:106-154.
Issa NP, Trepel C, Stryker MP (2000) Spatial frequency maps in cat visual cortex. J Neurosci 20:8504-8514.
Jammalamadaka SR, Sengupta A (2001) Topics in Circular Statistics.: World Scientific Publishing Company.
Juavinett AL, Callaway EM (2015) Pattern and Component Motion Responses in Mouse Visual Cortical Areas. Curr Biol 25:1759-1764.

Landy MS, Graham N (2004) Visual perception of texture. In: The Visual Neurosciences (Chalupa LM, Werner JS, eds): Cambridge, MA: MIT.
Leventhal AG, Wang Y, Schmolesky MT, Zhou Y (1998) Neural correlates of boundary perception. Vis Neurosci 15:1107-1118.
Levitt JB, Kiper DC, Movshon JA (1994) Receptive fields and functional architecture of macaque V2. J Neurophysiol 71:2517-2542.
Li G, Baker CL, Jr. (2012) Functional organization of envelope-responsive neurons in early visual cortex: organization of carrier tuning properties. J Neurosci 32:7538-7549.
Li G, Yao Z, Wang Z, Yuan N, Talebi V, Tan J, Wang Y, Zhou Y, Baker CL, Jr. (2014) Form-cue invariant second-order neuronal responses to contrast modulation in primate area V2. J Neurosci 34:12081-12092.
Liu B-h, Li P, Li Y-t, Sun YJ, Yanagawa Y, Obata K, Zhang LI, Tao HW (2009a) Visual Receptive Field Structure of Cortical Inhibitory Neurons Revealed by Two-Photon Imaging Guided Recording. Journal of Neuroscience 29:10520-10532.
Liu BH, Li P, Sun YJ, Li YT, Zhang LI, Tao HW (2009b) Intervening inhibition underlies simple-cell receptive field structure in visual cortex. Nat Neurosci 13:89-96.
Logothetis NK, Sheinberg DL (1996) Visual object recognition. Annu Rev Neurosci 19:577-621.
Mareschal I, Baker CL, Jr. (1998a) A cortical locus for the processing of contrast-defined contours. Nat Neurosci 1:150-154.
Mareschal I, Baker CL, Jr. (1998b) Temporal and spatial response to second-order stimuli in cat area 18. J Neurophysiol 80:2811-2823.
Mareschal I, Baker CL, Jr. (1999a) Cortical processing of second-order motion. Vis Neurosci 16:527-540.
Mareschal I, Baker CL, Jr. (1999b) Cortical processing of second-order motion. Vis Neurosci 16:527-540.
Marshel JH, Garrett ME, Nauhaus I, Callaway EM (2011) Functional Specialization of Seven Mouse Visual Cortical Areas. Neuron 72:1040--1054.
Mentis GZ, Blivis D, Liu W, Drobac E, Crowder ME, Kong L, Alvarez FJ, Sumner CJ, O'Donovan MJ (2011) Early Functional Impairment of Sensory-Motor Connectivity in a Mouse Model of Spinal Muscular Atrophy. Neuron 69:453-467.
Mishkin M, Ungerleider LG (1982) Contribution of striate inputs to the visuospatial functions of parieto-preoccipital cortex in monkeys. Behav Brain Res 6:57-77.
Movshon JA, Thompson ID, Tolhurst DJ (1978a) Spatial and temporal contrast sensitivity of neurones in areas 17 and 18 of the cat's visual cortex. J Physiol 283:101-120.
Movshon JA, Thompson ID, Tolhurst DJ (1978b) Spatial and temporal contrast sensitivity of neurones in areas 17 and 18 of the cat's visual cortex. The Journal of Physiology Online 283:101-120.
Niell CM, Stryker MP (2008a) Highly Selective Receptive Fields in Mouse Visual Cortex. J Neurosci 28:7520-7536.
Niell CM, Stryker MP (2008b) Highly Selective Receptive Fields in Mouse Visual Cortex. J Neurosci 28:7520-7536.
Pasupathy A, Connor CE (1999) Responses to Contour Features in Macaque Area V4. J Neurophysiol 82:2490-2502.
Peters AJ, Chen SX, Komiyama T (2014) Emergence of reproducible spatiotemporal activity during motor learning. Nature 510:263-267.

Poort J, Raudies F, Wannig A, Lamme VAF, Neumann H, Roelfsema PR (2012) The Role of Attention in Figure-Ground Segregation in Areas V1 and V4 of the Visual Cortex. Neuron 75:143--156.
Poort J, Khan AG, Pachitariu M, Nemri A, Orsolic I, Krupic J, Bauza M, Sahani M, Keller GB, Mrsic-Flogel TD, Hofer SB (2015) Learning Enhances Sensory and Multiple Non-sensory Representations in Primary Visual Cortex. Neuron 86:1478-1490.
Price DJ, Ferrer JM, Blakemore C, Kato N (1994) Functional organization of corticocortical projections from area 17 to area 18 in the cat's visual cortex. J Neurosci 14:2732-2746.
Quiroga RQ, Nadasdy Z, Ben-Shaul Y (2004) Unsupervised spike detection and sorting with wavelets and superparamagnetic clustering. Neural Comput 16:1661-1687.
R Development Core Team (2015) R: A Language and Environment for Statistical Computing. In. Vienna, Austria: R Foundation for Statistical Computing.
Ringach DL, Shapley RM, Hawken MJ (2002) Orientation Selectivity in Macaque V1: Diversity and Laminar Dependence. J Neurosci 22:5639-5651.
Rosenberg A, Issa NP (2011) The Y cell visual pathway implements a demodulating nonlinearity. Neuron 71:348-361.
Rosenberg A, Husson TR, Issa NP (2010) Subcortical representation of non-Fourier image features. J Neurosci 30:1985-1993.
Rust NC, DiCarlo JJ (2010) Selectivity and Tolerance ("Invariance") Both Increase as Visual Information Propagates from Cortical Area V4 to IT. Journal of Neuroscience 30:12978--12995.
Sacco T, Sacchetti B (2010) Role of secondary sensory cortices in emotional memory storage and retrieval in rats. Science 329:649-656.
Sary G, Vogels R, Orban GA (1993) Cue-invariant shape selectivity of macaque inferior temporal neurons. Science 260:995-997.
Schwartz EL, Desimone R, Albright TD, Gross CG (1983) Shape recognition and inferior temporal neurons. Proc Natl Acad Sci U S A 80:5776-5778.
Schwarz C, Hentschke H, Butovas S, Haiss F, Stüttgen MC, Gerdjikov TV, Bergner CG, Waiblinger C (2010) The head-fixed behaving rat---Procedures and pitfalls. Somatosensory \& Motor Research 27:131--148.
Smith SL, Hausser M (2010) Parallel processing of visual space by neighboring neurons in mouse visual cortex. Nat Neurosci 13:1144--1149.
Song Y, Baker CL, Jr. (2007) Neuronal response to texture- and contrast-defined boundaries in early visual cortex. Vis Neurosci 24:65-77.
Super H, Roelfsema PR (2005) Chronic multiunit recordings in behaving animals: advantages and limitations. Prog Brain Res 147:263-282.
Tanaka H, Ohzawa I (2009) Surround Suppression of V1 Neurons Mediates Orientation-Based Representation of High-Order Visual Features. J Neurophysiol 101:1444-1462.
Tanaka K (1996) Inferotemporal cortex and object vision. Annu Rev Neurosci 19:109-139.
Ungerleider LG, Haxby JV (1994) 'What' and 'where' in the human brain. Curr Opin Neurobiol 4:157-165.
Vaiceliunaite A, Erisken S, Franzen F, Katzner S, Busse L (2013) Spatial integration in mouse primary visual cortex. Journal of Neurophysiology 110:964-972.
Van den Bergh G, Zhang B, Arckens L, Chino YM (2010) Receptive-field properties of V1 and V2 neurons in mice and macaque monkeys. The Journal of Comparative Neurology 518:2051-2070.

van der Togt C, Spekreijse H, Supèr H (2005) Neural responses in cat visual cortex reflect state changes in correlated activity. European Journal of Neuroscience 22:465-475.
Vermaercke B, Van den Bergh G, Gerich F, Op de Beeck H (2015) Neural discriminability in rat lateral extrastriate cortex and deep but not superficial primary visual cortex correlates with shape discriminability. Front Neural Circuits 9:24.
Wang Q, Burkhalter A (2007) Area map of mouse visual cortex. The Journal of Comparative Neurology 502:339-357.
Wang Q, Burkhalter A (2013) Stream-related preferences of inputs to the superior colliculus from areas of dorsal and ventral streams of mouse visual cortex. J Neurosci 33:1696-1705.
Wang Q, Gao E, Burkhalter A (2011) Gateways of Ventral and Dorsal Streams in Mouse Visual Cortex. Journal of Neuroscience 31:1905-1918.
Wang Q, Sporns O, Burkhalter A (2012) Network Analysis of Corticocortical Connections Reveals Ventral and Dorsal Processing Streams in Mouse Visual Cortex. The Journal of Neuroscience 32:4386--4399.
Wickersham IR, Lyon DC, Barnard RJ, Mori T, Finke S, Conzelmann KK, Young JA, Callaway EM (2007) Monosynaptic restriction of transsynaptic tracing from single, genetically targeted neurons. Neuron 53:639-647.
Willmore BDB, Prenger RJ, Gallant JL (2010) Neural Representation of Natural Images in Visual Area V2. Journal of Neuroscience 30:2102-2114.
Zhan CA, Baker CL, Jr. (2006) Boundary cue invariance in cortical orientation maps. Cereb Cortex 16:896-906.
Zhou YX, Baker CL, Jr. (1993) A processing stream in mammalian visual cortex neurons for non-Fourier responses. Science 261:98-101.
Zhou YX, Baker CL, Jr. (1994) Envelope-responsive neurons in areas 17 and 18 of cat. J Neurophysiol 72:2134-2150.